Journal of Sound and Vibration (1999) **226**(3), 519–547
Article No. jsvi.1999.2308, available online at http://www.idealibrary.com on IDEAL®

HYBRID FINITE ELEMENT MODELS FOR PIEZOELECTRIC MATERIALS†

K. Y. SZE

Department of Mechanical Engineering, The University of Hong Kong, Pokfulam Road, Hong Kong, People's Republic of China

AND

Y. S. PAN

Institute of Computational Engineering Sciences, Southwest Jiatong University, Chengdu 10031, *People's Republic of China*

(*Received* 22 *July* 1998, *and in final form* 26 *March* 1999)

In this paper, hybrid variational principles are employed for piezoelectric finite element formulation. Starting from eight-node hexahedral elements with displacement and electric potential as the nodal d.o.f.s, hybrid models with assumed stress and electric displacement are devised. The assumed stress and electric displacement are chosen to be contravariant with the minimal 18 and seven modes respectively. The pertinent coefficients can be condensed at the element level and do not enter the system equation. A number of benchmark tests are exercised. The predicted results indicate that the assumed stress and electric displacements are effective in improving the element accuracy.

1. INTRODUCTION

Piezoelectric materials have been indispensable for electrochemical resonators, transducers, sensors, actuators and adaptive structures. Owing to the complexity of the governing equations in piezoelectricity, only a few simple problems such as simply supported beams and plates can be solved analytically [1–4]. Since Allik and Hughes [5] presented their work on finite element (f.e.) method for piezoelectric vibration analysis, the method has been the dominating practical tool for design and analysis of piezoelectric devices and adaptive structures. Inheriting Allik and Hughes' work, all of the f.e. models presented in references [6–22] include displacement and electric potential as the only assumed field variables. Other fields such as stress, electric displacement, etc., are derived from displacement and electric potential. These models and the associated formulation can be classified as irreducible in the sense that the number of field variables cannot be further reduced

†This work was conducted when the second author was visiting the University of Hong Kong as a research associate.

0022-460X/99/380519 + 29 $30.00/0

[23]. Same as the irreducible or displacement elements in structural mechanics, irreducible piezoelectric elements are often too stiff, susceptible to mesh distortion and aspect ratio. To overcome these drawbacks, Tzou and Tseng [14], Ha *et al.* [16] and Tzou [17] made use of bubble/incompatible displacement modes [24, 25] to improve the eight-node hexahedral element.

In addition to the bubble/incompatible displacement method hybrid (or reducible) variational principles in structural mechanics have been successfully employed for enhancing the element accuracy and circumventing various locking phenomena [26–41]. In this light, Ghandi and Hagood [42] have proposed a piezoelectric hybrid tetrahedral finite element model in which electric displacement, electric potential and displacement are assumed. Their model is markedly superior to the irreducible model. Besides reference [42], hybrid variational principles have rarely been used in formulating piezoelectric finite element models.

In this paper, we shall start with a general hybrid variational principle that contains stress, strain, displacement, electric displacement, electric field and electric potential as the independently assumed field variables. It will be seen that the stationary conditions of the functional are the nine governing equations in linear piezoelectricity. For domain decomposition methods such as the f.e. method, the prerequisities and the continuity requirements on the field variables assumed in the principle are addressed. Four degenerated versions of the general principle are adopted for f.e. formulation. Judging from the results obtained for a number of benchmark problems, the proposed hybrid models are more accurate than the irreducible ones.

2. GOVERNING EQUATIONS IN LINEAR PIEZOELECTRICITY

For a solid piezoelectric body occupying domain Ω, the governing equations are summarized below [43, 44].

(i) strain–displacement relation: $\boldsymbol{\gamma} = \mathscr{D}_m \mathbf{u} \quad \text{in } \Omega;$ (1)

(ii) electric field–electric potential relation: $\mathbf{E} = -\mathscr{D}_e \phi \quad \text{in } \Omega;$ (1b)

(iii) constitutive relations: $\begin{Bmatrix} \boldsymbol{\tau} \\ \mathbf{D} \end{Bmatrix} = \begin{bmatrix} \mathbf{c}_E & -\mathbf{e}^{\mathrm{T}} \\ \mathbf{e} & \boldsymbol{\varepsilon}_\gamma \end{bmatrix} \begin{Bmatrix} \boldsymbol{\gamma} \\ \mathbf{E} \end{Bmatrix} \quad \text{in } \Omega;$ (1c)

(iv) stress equilibrium condition: $\mathscr{D}_m^{\mathrm{T}} \boldsymbol{\tau} + \mathbf{b} = \mathbf{0} \quad \text{in } \Omega;$ (1d)

(v) charge conservation condition: $\mathscr{D}_e^{\mathrm{T}} \mathbf{D} = \mathbf{0} \quad \text{in } \Omega;$ (1e)

(vi) mechanical natural boundary condition: $\mathbf{n}_m \boldsymbol{\tau} = \bar{\mathbf{t}} \quad \text{on } S_t;$ (1f)

(vii) electric natural boundary condition: $\mathbf{n}_e\mathbf{D} = \bar{\omega}$ on S_ω; (1g)

(viii) mechanical essential boundary condition: $\mathbf{u} = \bar{\mathbf{u}}$ on S_u; (1h)

(ix) electrical essential boundary condition: $\phi = \bar{\phi}$ on S_ϕ; (1i)

where $\boldsymbol{\gamma} = \{\gamma_{xx}, \gamma_{yy}, \gamma_{zz}, 2\gamma_{xy}, 2\gamma_{yz}, 2\gamma_{zx}\}^{\mathrm{T}}$ is the vector of strain components, $\mathbf{u} = \{u_x, u_y, u_z\}^{\mathrm{T}}$ is the displacement, $\mathbf{E} = \{E_x, E_y, E_z\}^{\mathrm{T}}$ is the electric field, $\boldsymbol{\tau} = \{\tau_{xx}, \tau_{yy}, \tau_{zz}, \tau_{xy}, \tau_{yz}, \tau_{zz}\}^{\mathrm{T}}$ is the vector of stress components, $\mathbf{D} = \{D_x, D_y, D_z\}^{\mathrm{T}}$ is the electric displacement, $\bar{\mathbf{b}} = \{\bar{b}_x, \bar{b}_y, \bar{b}_z\}^{\mathrm{T}}$ is the boy force, $\bar{\mathbf{t}} = \{\bar{t}_x, \bar{t}_y, \bar{t}_z\}^{\mathrm{T}}$ is the prescribed traction, $\bar{\mathbf{u}} = \{\bar{u}_x, \bar{u}_y, \bar{u}_z\}^{\mathrm{T}}$ is the prescribed displacement, $\mathbf{c}_E = \mathbf{c}_E^{\mathrm{T}}$ is the elasticity matrix measured at constant electric field, $\mathbf{e}$ is the piezoelectric matrix measured at constant strain, $\boldsymbol{\varepsilon}_\gamma = \boldsymbol{\varepsilon}_\gamma^{\mathrm{T}}$ is the dielectric matrix measured at constant strain,

$$\mathscr{D}_e = \begin{bmatrix} \partial/\partial x \\ \partial/\partial y \\ \partial/\partial z \end{bmatrix}, \quad \mathscr{D}_m = \begin{bmatrix} \partial/\partial x & 0 & 0 & \partial/\partial y & 0 & \partial/z \\ 0 & \partial/\partial y & 0 & \partial/x & \partial/\partial z & 0 \\ 0 & 0 & \partial/\partial z & 0 & \partial/\partial y & \partial/\partial x \end{bmatrix}^{\mathrm{T}},$$

$$\mathbf{n}_m = \begin{bmatrix} n_x & 0 & 0 & n_y & 0 & n_z \\ 0 & n_y & 0 & n_x & n_z & 0 \\ 0 & 0 & n_z & 0 & n_y & n_x \end{bmatrix}, \quad \mathbf{n}_e = \begin{bmatrix} n_x & 0 & 0 \\ 0 & n_y & 0 \\ 0 & 0 & n_z \end{bmatrix},$$

$\{n_x, n_y, n_z\}^{\mathrm{T}}$ is the unit outward normal vector to the boundary $\partial\Omega$ of domain Ω.

It will be assumed as usual that the boundary $\partial\Omega$ of the domain Ω can be partitioned according to the boundary conditions into S_t, S_u, S_ω and S_ϕ such that

$$S_t \cap S_u = S_\omega \cap S_\phi = \text{null}, \quad S_t \cup S_u = S_\omega \cup S_\phi = \partial\Omega. \tag{2}$$

It is noteworthy that $\boldsymbol{\gamma}$ and $-\mathbf{E}$ are the energy conjugates of $\boldsymbol{\tau}$ and $\mathbf{D}$ respectively. By changing the objects in the constitutive relations, the following alternate forms can be obtained:

$$\begin{Bmatrix} \boldsymbol{\gamma} \\ \mathbf{E} \end{Bmatrix} = \begin{bmatrix} \mathbf{c}_E & -\mathbf{e}^{\mathrm{T}} \\ \mathbf{e} & \boldsymbol{\varepsilon}_\varepsilon \end{bmatrix}^{-1} \begin{Bmatrix} \boldsymbol{\tau} \\ \mathbf{D} \end{Bmatrix} = \begin{bmatrix} \mathbf{s}_D & \mathbf{g}^{\mathrm{T}} \\ -\mathbf{g} & \mathbf{f}_\sigma \end{bmatrix} \begin{Bmatrix} \boldsymbol{\tau} \\ \mathbf{D} \end{Bmatrix}, \tag{3a}$$

$$\begin{Bmatrix} \boldsymbol{\tau} \\ \mathbf{E} \end{Bmatrix} = \begin{bmatrix} \mathbf{c}_E + \mathbf{e}^{\mathrm{T}}\boldsymbol{\varepsilon}_\gamma^{-1}\mathbf{e} & -(\boldsymbol{\varepsilon}_\gamma^{-\mathrm{T}}\mathbf{e})^{\mathrm{T}} \\ -\boldsymbol{\varepsilon}_\gamma^{-\mathrm{T}}\mathbf{e} & \mathbf{f}_\gamma \end{bmatrix} \begin{Bmatrix} \boldsymbol{\gamma} \\ \mathbf{D} \end{Bmatrix} = \begin{bmatrix} \mathbf{c}_D & -\mathbf{h}^{\mathrm{T}} \\ -\mathbf{h} & \mathbf{f}_\gamma \end{bmatrix} \begin{Bmatrix} \boldsymbol{\gamma} \\ \mathbf{D} \end{Bmatrix}. \tag{3b}$$

3. A GENERAL VARIATIONAL PRINCIPLE FOR PIEZOELECTRICITY

A few researchers have investigated the variational principles for piezoelectric bodies [43, 44]. The most general variational principle that includes all the six

assumed field variables is

$$\Pi_G = \int_\Omega \left[\frac{1}{2} \begin{Bmatrix} \boldsymbol{\gamma} \\ -\mathbf{E} \end{Bmatrix}^{\mathrm{T}} \begin{bmatrix} \mathbf{c}_E & \mathbf{e}^{\mathrm{T}} \\ \mathbf{e} & -\boldsymbol{\varepsilon}_\gamma \end{bmatrix} \begin{Bmatrix} \boldsymbol{\gamma} \\ -\mathbf{E} \end{Bmatrix} - \begin{Bmatrix} \boldsymbol{\tau} \\ \mathbf{D} \end{Bmatrix}^{\mathrm{T}} \left(\begin{Bmatrix} \boldsymbol{\gamma} \\ -\mathbf{E} \end{Bmatrix} - \begin{Bmatrix} \mathscr{D}_m \mathbf{u} \\ \mathscr{D}_e \phi \end{Bmatrix} \right) - \bar{\mathbf{b}}^{\mathrm{T}} \mathbf{u} \right] \mathrm{d}v$$

$$- \int_{S_t} \bar{\mathbf{t}}^{\mathrm{T}} \mathbf{u} \, \mathrm{d}s - \int_{S_\omega} \phi \bar{\omega} \, \mathrm{d}s - \int_{S_u} (\mathbf{n}_m \boldsymbol{\tau})^{\mathrm{T}} (\mathbf{u} - \bar{\mathbf{u}}) \, \mathrm{d}s - \int_{S_\phi} (\mathbf{n}_e \mathbf{D})^{\mathrm{T}} (\phi - \bar{\phi}) \, \mathrm{d}s, \tag{4}$$

where

$$\frac{1}{2} \begin{Bmatrix} \boldsymbol{\gamma} \\ -\mathbf{E} \end{Bmatrix}^{\mathrm{T}} \begin{bmatrix} \mathbf{c}_E & \mathbf{e}^{\mathrm{T}} \\ \mathbf{e} & -\boldsymbol{\varepsilon}_\gamma \end{bmatrix} \begin{Bmatrix} \boldsymbol{\gamma} \\ -\mathbf{E} \end{Bmatrix} = H(\boldsymbol{\gamma}, -\mathbf{E})$$

is known as the electric enthalpy. By recalling the divergence theorems, we have

$$\int_\Omega (\delta \mathbf{u} \mathscr{D}_m^{\mathrm{T}} \boldsymbol{\tau} + \boldsymbol{\tau}^{\mathrm{T}} \mathscr{D}_m \delta \mathbf{u}) \, \mathrm{d}v = \int_{\partial\Omega} (\mathbf{n}_m \boldsymbol{\tau})^{\mathrm{T}} \delta \mathbf{u} \, \mathrm{d}s, \tag{5a}$$

$$\int_\Omega (\delta \phi \mathscr{D}_e^{\mathrm{T}} \mathbf{D} + \mathbf{D}^{\mathrm{T}} \mathscr{D}_e \delta \phi) \, \mathrm{d}v = \int_{\partial\Omega} (\mathbf{n}_e \mathbf{D})^{\mathrm{T}} \delta \phi \, \mathrm{d}s, \tag{5b}$$

in which δ is the variational symbol. Variation of Π_G can then be worked out as

$$\delta \Pi_G = \int_\Omega \left[\begin{Bmatrix} \delta \boldsymbol{\gamma} \\ -\delta \mathbf{E} \end{Bmatrix}^{\mathrm{T}} \left(\begin{bmatrix} \mathbf{c}_E & \mathbf{e}^{\mathrm{T}} \\ \mathbf{e} & -\boldsymbol{\varepsilon}_\gamma \end{bmatrix} \begin{Bmatrix} \boldsymbol{\gamma} \\ -\mathbf{E} \end{Bmatrix} - \begin{Bmatrix} \boldsymbol{\tau} \\ \mathbf{D} \end{Bmatrix} \right) - \begin{Bmatrix} \delta \boldsymbol{\tau} \\ \delta \mathbf{D} \end{Bmatrix}^{\mathrm{T}} \left(\begin{Bmatrix} \boldsymbol{\gamma} \\ -\mathbf{E} \end{Bmatrix} - \begin{Bmatrix} \mathscr{D}_m \mathbf{u} \\ \mathscr{D}_e \phi \end{Bmatrix} \right)$$

$$- \begin{Bmatrix} \delta \mathbf{u} \\ \delta \phi \end{Bmatrix}^{\mathrm{T}} \begin{Bmatrix} \mathscr{D}_m^{\mathrm{T}} \boldsymbol{\tau} + \bar{\mathbf{b}} \\ \mathscr{D}_e^{\mathrm{T}} \mathbf{D} \end{Bmatrix} \Bigg] \mathrm{d}v + \int_{S_t} (\mathbf{n}_e \boldsymbol{\tau} - \bar{\mathbf{t}})^{\mathrm{T}} \delta \mathbf{u} \, \mathrm{d}s + \int_{S_\omega} (\mathbf{n}_e \mathbf{D} - \bar{\omega}) \delta \phi \, \mathrm{d}s$$

$$- \int_{S_u} (\mathbf{n}_m \delta \boldsymbol{\tau})^{\mathrm{T}} (\mathbf{u} - \bar{\mathbf{u}}) \, \mathrm{d}s - \int_{S_\phi} (\mathbf{n}_e \delta \mathbf{D})^{\mathrm{T}} (\phi - \bar{\phi}) \, \mathrm{d}s. \tag{6}$$

The generalization of the functional can be seen as its Euler's equations include all the nine governing equations in equation (1).

4. DOMAIN DECOMPOSITION

We now consider the piezoelectric domain Ω be decomposed into two subdomains Ω^1 and Ω^2 as shown in Figure 1. Let superscripts be used for subdomain designation and S_{12} be the subdomain interfacial for Ω^1 and Ω^2, it will be assumed that

$$S_t^1 \cup S_t^2 = S_t, \quad S_u^1 \cup S_u^2 = S_u, \quad S_\omega^1 \cup S_\omega^2 = S_\omega, \quad S_\phi^1 \cup S_\phi^2 = S_\phi. \tag{7a}$$

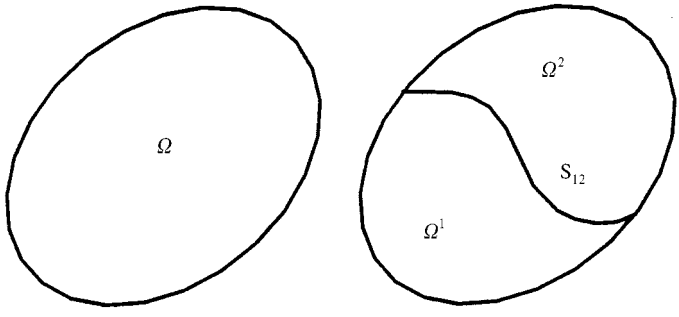

Figure 1. A piezoelectric domain Ω (left) and it sub-domain Ω^1 and Ω^2 (right), S_{12} is the sub-domain interface.

Moreover,

$$\Omega^1 \cup \Omega^2 = \Omega, \quad S_t^i \cup S_u^i \cup S_{12} = S_\omega^i \cup S_\phi^i \cup S_{12} = \partial\Omega^i \quad \text{for } i = 1, 2. \tag{7b}$$

The governing equations after decomposing the domain are

$$\text{(i) } \boldsymbol{\gamma}^i = \mathscr{D}_m \mathbf{u}^i \quad \text{in } \Omega^i, \quad \text{(ii) } \mathbf{E}^i = -\mathscr{D}_e \phi^i \quad \text{in } \Omega^i,$$

$$\text{(iii) } \begin{Bmatrix} \boldsymbol{\tau}^i \\ \mathbf{D}^i \end{Bmatrix} = \begin{bmatrix} \mathbf{c}_E^i & -(\mathbf{e}^i)^{\mathrm{T}} \\ \mathbf{e}^i & -\boldsymbol{\varepsilon}_\gamma^i \end{bmatrix} \begin{Bmatrix} \boldsymbol{\gamma}^i \\ \mathbf{E}^i \end{Bmatrix} \quad \text{in } \Omega^i, \tag{8a}$$

$$\text{(iv) } \mathscr{D}_m^{\mathrm{T}} \boldsymbol{\tau}^i + \bar{\mathbf{b}} = \mathbf{0} \quad \text{in } \Omega^i, \quad \text{(v) } \mathscr{D}_e^{\mathrm{T}} \mathbf{D}^i = \mathbf{0}, \quad \text{in } \Omega^i, \quad \text{(vi) } \mathbf{n}_m^i \boldsymbol{\tau}^i = \bar{\mathbf{t}} \quad \text{on } S_t^i, \tag{8b}$$

$$\text{(vii) } \mathbf{n}_e^i \mathbf{D}^i = \bar{\omega} \quad \text{on } S_\omega^i, \quad \text{(viii) } \mathbf{u}^i = \bar{\mathbf{u}} \quad \text{on } S_u^i, \quad \text{(ix) } \phi^i = \bar{\phi} \quad \text{on } S_\phi^i, \tag{8c}$$

$$\text{(x) mechanical reciprocity condition: } \mathbf{n}_m^1 \boldsymbol{\tau}^1 + \mathbf{n}_m^2 \boldsymbol{\tau}^2 = \mathbf{0} \quad \text{on } S_{12}, \tag{8d}$$

$$\text{(xi) electric reciprocity condition: } \mathbf{n}_e^1 \mathbf{D}^1 + \mathbf{n}_e^2 \mathbf{D}^2 = 0 \quad \text{on } S_{12}, \tag{8e}$$

$$\text{(xii) mechanical compatibility condition: } u^1 = \mathbf{u}^2 \quad \text{on } S_{12}, \tag{8f}$$

$$\text{(xiii) electric compatibility condition: } \phi^1 = \phi^2 \quad \text{on } S_{12} \tag{8g}$$

for $i = 1$ and 2. Compared to equation (1), there are four extra conditions to be satisfied on the subdomain interface S_{12}. With $\Omega = \Omega^1 \cup \Omega^2$, Π_G in equation (4) can be expressed as

$$\Pi_G = \Pi_G^1 + \Pi_G^2, \tag{9}$$

where

$$\Pi_G^i = \int_{\Omega^i} \left[\frac{1}{2} \begin{Bmatrix} \boldsymbol{\gamma}^i \\ -\mathbf{E}^i \end{Bmatrix}^{\mathrm{T}} \begin{bmatrix} \mathbf{c}_E^i & (\mathbf{e}^i)^{\mathrm{T}} \\ \mathbf{e}^i & -\boldsymbol{\varepsilon}_\gamma^i \end{bmatrix} \begin{Bmatrix} \boldsymbol{\gamma}^i \\ -\mathbf{E}^i \end{Bmatrix} - \begin{Bmatrix} \boldsymbol{\tau}^i \\ \mathbf{D}^i \end{Bmatrix}^{\mathrm{T}} \left(\begin{Bmatrix} \boldsymbol{\gamma}^i \\ -\mathbf{E}^i \end{Bmatrix} - \begin{Bmatrix} \mathscr{D}_m \mathbf{u}^i \\ \mathscr{D}_e \phi^i \end{Bmatrix} \right) - (\bar{\mathbf{b}})^{\mathrm{T}} \mathbf{u}^i \right] \mathrm{d}v$$

$$- \int_{S_t^i} \bar{\mathbf{t}}^{\mathrm{T}} \mathbf{u}^i \, \mathrm{d}s - \int_{S_\omega^i} \phi^i \bar{\omega} \, \mathrm{d}s - \int_{S_u^i} (\mathbf{n}_m^i \boldsymbol{\tau}^i)^{\mathrm{T}} (\mathbf{u}^i - \bar{\mathbf{u}}) \, \mathrm{d}s - \int_{S_\phi^i} (\mathbf{n}_e^i \mathbf{D}^i)^{\mathrm{T}} (\phi^i - \bar{\phi}) \, \mathrm{d}s.$$

By invoking equation (5) and (7),

$$\delta \Pi_G = \sum_{i=1}^{2} \left(\int_{\Omega^i} \left[\begin{Bmatrix} \delta \boldsymbol{\gamma}^i \\ -\delta \mathbf{E}^i \end{Bmatrix}^{\mathrm{T}} \left(\begin{bmatrix} \mathbf{c}_E^i & (\mathbf{e}^i)^{\mathrm{T}} \\ \mathbf{e}^i & -\boldsymbol{\varepsilon}_\gamma^i \end{bmatrix} \begin{Bmatrix} \boldsymbol{\gamma}^i \\ -\mathbf{E}^i \end{Bmatrix} - \begin{Bmatrix} \boldsymbol{\tau}^i \\ \mathbf{D}^i \end{Bmatrix} \right) - \begin{Bmatrix} \delta \boldsymbol{\tau}^i \\ \delta \mathbf{D}^i \end{Bmatrix}^{\mathrm{T}} \right.$$

$$\times \left(\begin{Bmatrix} \boldsymbol{\gamma}^i \\ -\mathbf{E}^i \end{Bmatrix} - \begin{Bmatrix} \mathscr{D}_m \mathbf{u}^i \\ \mathscr{D}_e \phi^i \end{Bmatrix} \right) \Bigg] \mathrm{d}v - \int_{\Omega^i} \begin{Bmatrix} \delta \mathbf{u}^i \\ \delta \phi^i \end{Bmatrix}^{\mathrm{T}} \begin{Bmatrix} \mathscr{D}_m^{\mathrm{T}} \boldsymbol{\tau}^i - \bar{\mathbf{b}} \\ \mathscr{D}_e^{\mathrm{T}} \mathbf{D}^i \end{Bmatrix} \mathrm{d}v$$

$$+ \int_{S_t^i} (\mathbf{n}_m^i \boldsymbol{\tau}^i - \bar{\mathbf{t}})^{\mathrm{T}} \delta \mathbf{u}^i \, \mathrm{d}s + \int_{S_\omega^i} (\mathbf{n}_e^i \mathbf{D}^i - \bar{\omega}) \delta \phi^i \, \mathrm{d}s - \int_{S_u^i} (\mathbf{n}_m^i \delta \boldsymbol{\tau}^i)^{\mathrm{T}} (\mathbf{u}^i - \bar{\mathbf{u}}) \, \mathrm{d}s$$

$$\left. - \int_{S_\phi^i} (\mathbf{n}_e^i \delta \mathbf{D}^i)^{\mathrm{T}} (\phi^i - \bar{\phi}) \, \mathrm{d}s + \int_{S_{12}} [(\mathbf{n}_m^i \boldsymbol{\tau}^i)^{\mathrm{T}} \delta \mathbf{u}^i + (\mathbf{n}_e^i \mathbf{D}^i) \delta \phi^i] \, \mathrm{d}s \right). \tag{10}$$

By constraining the two compatibility conditions, we have

$$\mathbf{u}^1 = \mathbf{u}^2, \quad \delta \mathbf{u}^1 = \delta \mathbf{u}^2, \quad \phi^1 = \phi^2 \quad \text{and} \quad \delta \phi^1 = \delta \phi^2 \quad \text{on } S_{12}, \tag{11}$$

with which the last term in $\delta \Pi_G$ can be expressed as

$$\sum_{i=1}^{2} \int_{S_{12}} [(n_m^i \boldsymbol{\tau}^i)^{\mathrm{T}} \delta \mathbf{u}^i + (\mathbf{n}_e^i D^i) \delta \phi^i] \, \mathrm{d}s = \int_{S_{12}} [(\mathbf{n}_m^1 \boldsymbol{\tau}^1 + \mathbf{n}_m^2 \boldsymbol{\tau}^2)^{\mathrm{T}} \delta \mathbf{u}^1 + (\mathbf{n}_e^1 \mathbf{D}^1 + \mathbf{n}_e^2 \mathbf{D}^2) \delta \phi^1] \, \mathrm{d}s. \tag{12}$$

Hence, with the two compatibility conditions satisfied as *a priori*, Euler's equations of Π_G include the first 11 conditions in equation (8). In other words, zeroth order continuity of the displacement and electric potential at the subdomain interface must be ensured when Π_G is employed. There is no continuity requirement on the other field variables at the subdomain interface, i.e., the two sets of field variables in the two subdomains can be totally independent of each other. The arguments presented here can readily be generalized to multiply subdomains such as in f.e. meshes.

5. DEGENERATED VARIATIONAL PRINCIPLES

In the f.e. method, the two essential boundary conditions can be satisfied by having displacement and electric potential as the nodal variables. With the two

conditions constrained, Π_G is simplified to

$$\Pi_{mG} = \int_\Omega \left[\frac{1}{2} \begin{Bmatrix} \boldsymbol{\gamma} \\ -\mathbf{E} \end{Bmatrix}^{\mathrm{T}} \begin{bmatrix} \mathbf{c}_E & \mathbf{e}^{\mathrm{T}} \\ \mathbf{e} & -\boldsymbol{\varepsilon}_\gamma \end{bmatrix} \begin{Bmatrix} \boldsymbol{\gamma} \\ -\mathbf{E} \end{Bmatrix} - \begin{Bmatrix} \boldsymbol{\tau} \\ \mathbf{D} \end{Bmatrix}^{\mathrm{T}} \left(\begin{Bmatrix} \boldsymbol{\gamma} \\ -\mathbf{E} \end{Bmatrix} - \begin{Bmatrix} \mathscr{D}_m \mathbf{u} \\ \mathscr{D}_e \phi \end{Bmatrix} \right) - \bar{\mathbf{b}}^{\mathrm{T}} \mathbf{u} \right] \mathrm{d}v$$

$$- \int_{S_t} \bar{\mathbf{t}}^{\mathrm{T}} \mathbf{u} \, \mathrm{d}s - \int_{S_\omega} \phi \bar{\omega} \, \mathrm{d}S_\phi. \tag{13}$$

In this paper, four variation functionals having degenerated from Π_{mG} will be employed for finite element formulation.

(I) *Functional with only* $\mathbf{u}$ and ϕ *assumed*—With the electric field–potential relation $\mathbf{E} = -\mathscr{D}_e \phi$ and the strain–displacement relation $\boldsymbol{\gamma} = \mathscr{D}_m \mathbf{u}$ constrained, the assumed stress, strain, electric field and electric displacement can be eliminated from Π_{mG}. The resulting functional is

$$\Pi = \int_\Omega \left(\frac{1}{2} \begin{Bmatrix} \mathscr{D}_m \mathbf{u} \\ \mathscr{D}_e \phi \end{Bmatrix}^{\mathrm{T}} \begin{bmatrix} \mathbf{c}_E & \mathbf{e}^{\mathrm{T}} \\ \mathbf{e} & -\boldsymbol{\varepsilon}_\gamma \end{bmatrix} \begin{Bmatrix} \mathscr{D}_m \mathbf{u} \\ \mathscr{D}_e \phi \end{Bmatrix} - \bar{\mathbf{b}}^{\mathrm{T}} \mathbf{u} \right) \mathrm{d}v - \int_{S_t} \bar{\mathbf{t}}^{\mathrm{T}} \mathbf{u} \, \mathrm{d}s - \int_{S_\phi} \phi \bar{\omega} \, \mathrm{d}s. \tag{14}$$

This gives rise to the irreducible formulation in piezoelectricity [5, 23].

(II) *Functional with* D, $\mathbf{u}$ *and* ϕ *assumed*—With the strain–displacement relation $\boldsymbol{\gamma} = \mathscr{D}_m \mathbf{u}$ and the constitutive relation $\mathbf{D} = \mathbf{e}\boldsymbol{\gamma} + \boldsymbol{\varepsilon}_\gamma \mathbf{E}$ constrained, the assumed stress, strain and electric field can be eliminated from Π_{mG}. The resulting functional is

$$\Pi_D = \int_\Omega \left[\frac{1}{2} \begin{Bmatrix} \mathscr{D}_m \mathbf{u} \\ \mathbf{D} \end{Bmatrix}^{\mathrm{T}} \begin{bmatrix} \mathbf{c}_D & -\mathbf{h}^{\mathrm{T}} \\ -\mathbf{h} & -\mathbf{f}_\gamma \end{bmatrix} \begin{Bmatrix} \mathscr{D}_m \mathbf{u} \\ \mathbf{D} \end{Bmatrix} + \mathbf{D}^{\mathrm{T}} \mathscr{D}_e \phi - \bar{\mathbf{b}}^{\mathrm{T}} \mathbf{u} \right] \mathrm{d}v$$

$$- \int_{S_t} \bar{\mathbf{t}}^{\mathrm{T}} \mathbf{u} \, \mathrm{d}s - \int_{S_\omega} \phi \bar{\omega} \, \mathrm{d}s. \tag{15}$$

(III) *Functional with* $\boldsymbol{\tau}$, $\mathbf{u}$ *and* ϕ *assumed*—With the electric field–potential relation $\mathbf{E} = -\mathscr{D}_e \phi$ and the constitutive relation $\boldsymbol{\tau} \doteq \mathbf{c}_E \boldsymbol{\gamma} - \mathbf{e}^{\mathrm{T}} \mathbf{E}$ constrained, strain, electric field and electric displacement can be eliminated from Π_{mG}. The resulting functional is

$$\Pi_\tau = \int_\Omega \left(\frac{-1}{2} \begin{Bmatrix} \boldsymbol{\tau} \\ \mathscr{D}_e \phi \end{Bmatrix}^{\mathrm{T}} \begin{bmatrix} \mathbf{s}_E & -\mathbf{d} \\ -\mathbf{d} & \boldsymbol{\varepsilon}_\tau \end{bmatrix} \begin{Bmatrix} \boldsymbol{\tau} \\ \mathscr{D}_e \phi \end{Bmatrix} + \boldsymbol{\tau}^{\mathrm{T}} \mathscr{D}_m \mathbf{u} - \bar{\mathbf{b}}^{\mathrm{T}} \mathbf{u} \right) \mathrm{d}v - \int_{S_t} \bar{\mathbf{t}}^{\mathrm{T}} \mathbf{u} \, \mathrm{d}s$$

$$- \int_{S_\phi} \phi \bar{\omega} \, \mathrm{d}s. \tag{16}$$

(IV) *Functional with* $\boldsymbol{\tau}$, $\mathbf{D}$, $\mathbf{u}$ and ϕ assumed—With the constitutive relations $\boldsymbol{\tau} = \mathbf{c}_E \boldsymbol{\gamma} - \mathbf{e}^{\mathrm{T}} \mathbf{E}$ and $\mathbf{D} = \mathbf{e}\boldsymbol{\gamma} + \boldsymbol{\varepsilon}_\gamma \mathbf{E}$ constrained, the assumed strain and electric field

can be eliminate from Π_{mG}. The resulting functional is

$$\Pi_{D\tau} = \int_\Omega \left(\frac{-1}{2} \begin{Bmatrix} \boldsymbol{\tau} \\ \mathbf{D} \end{Bmatrix}^{\mathrm{T}} \begin{bmatrix} \mathbf{S}_D & \mathbf{g}^{\mathrm{T}} \\ \mathbf{g} & -\mathbf{f}_\tau \end{bmatrix} \begin{Bmatrix} \boldsymbol{\tau} \\ \mathbf{D} \end{Bmatrix} + \begin{Bmatrix} \boldsymbol{\tau} \\ \mathbf{D} \end{Bmatrix}^{\mathrm{T}} \begin{Bmatrix} \mathscr{D}_m \mathbf{u} \\ \mathscr{D}_e \phi \end{Bmatrix} - \bar{\mathbf{b}}^{\mathrm{T}} \mathbf{u} \right) \mathrm{d}v$$

$$- \int_{S_t} \bar{\mathbf{t}}^{\mathrm{T}} \mathbf{u} \, \mathrm{d}s - \int_{S_\omega} \phi \bar{\omega} \, \mathrm{d}s, \tag{17}$$

where

$$\frac{1}{2} \begin{Bmatrix} \boldsymbol{\tau} \\ \mathbf{D} \end{Bmatrix}^{\mathrm{T}} \begin{bmatrix} \mathbf{S}_D & \mathbf{g}^{\mathrm{T}} \\ \mathbf{g} & -\mathbf{f}_\tau \end{bmatrix} \begin{Bmatrix} \boldsymbol{\tau} \\ \mathbf{D} \end{Bmatrix} = M(\boldsymbol{\tau}, \mathbf{D}) \quad \text{is known as the mechanical enthalpy.}$$

Only assumed stress and/or electric displacement are considered in equations (15)–(17) in addition to assumed displacement and electric potential because the homogenous equilibrium and charge conservation conditions can readily be satisfied by manipulating the stress and electric displacement shape functions.

6. FINITE ELEMENT FORMULATION

Being degenerated version of Π_G, the prerequisites and continuity requirements on the field variables of Π, Π_D, Π_τ and $\Pi_{D\tau}$ are identical to those discussed in section 4. In other words, the two compatibility conditions must be satisfied *a priori*, whereas the assumed stress and electric displacement in each element can be independent of the ones in other elements. Zeroth order continuity of the displacement and electric potential can be met by having displacement and electric potential as the nodal d.o.f.s.

In section 4, superscripts are employed for subdomain designation. Superscripts of the field variables will here be dropped for simplicity. Within a generic element, the assumed field variables are discretized as

$$\mathbf{u} = \mathbf{N}_m \mathbf{q}_m, \quad \phi = \mathbf{N}_e \mathbf{q}_e, \quad \boldsymbol{\tau} = \mathbf{P}_m \boldsymbol{\beta}_m, \quad \mathbf{D} = \mathbf{P}_e \boldsymbol{\beta}_e, \tag{18}$$

in which $\mathbf{N}_m$ is the displacement interpolation matrix, $\mathbf{q}_m$ is the vector of element nodal displacement d.o.f.s, $\mathbf{N}_e$ is the electric potential interpolation matrix, $\mathbf{q}_e$ is the vector of element nodal electric potential d.o.f.s., $\mathbf{P}_m$ is the stress shape function matrix, $\boldsymbol{\beta}_m$ is the vector of stress coefficients, $\mathbf{P}_e$ is the electric displacement shape function matrix and $\boldsymbol{\beta}_e$ is the vector of electric displacement coefficients. Moreover, we define

$$\mathbf{B}_m = \mathscr{D}_m \mathbf{N}_m, \quad \mathbf{B}_e = \mathscr{D}_e \mathbf{N}_e. \tag{19}$$

It has been shown that $\boldsymbol{\tau}$ and $\mathbf{D}$ need not be continuous across the element interface. Thus, every element has its own coefficient vectors $\boldsymbol{\beta}_e$ and $\boldsymbol{\beta}_m$ which can be

condensed in the element level.

1. *Finite element formulation using* $\Pi = \sum_e \Pi^e$—the elementwise version of Π is

$$\Pi^e = \int_{\Omega^e} \left(\frac{1}{2} \begin{Bmatrix} \mathscr{D}_m \mathbf{u} \\ \mathscr{D}_e \phi \end{Bmatrix}^{\mathrm{T}} \begin{bmatrix} \mathbf{c}_E & \mathbf{e}^{\mathrm{T}} \\ \mathbf{e} & -\boldsymbol{\varepsilon}_\gamma \end{bmatrix} \begin{Bmatrix} \mathscr{D}_m \mathbf{u} \\ \mathscr{D}_e \phi \end{Bmatrix} - \bar{\mathbf{b}}^{\mathrm{T}} \mathbf{u} \right) \mathrm{d}v - P_S^e, \tag{20}$$

where Ω^e denotes the element domain and

$$P_S^e = \int_{S_t^e} \bar{\mathbf{t}}^{\mathrm{T}} \mathbf{u} \, \mathrm{d}s + \int_{S_\omega^e} \phi \bar{\omega} \, \mathrm{d}s,$$

denotes the surface load acting on the element. With equations (18) and (19) invoked

$$\Pi^e = \frac{1}{2} \begin{Bmatrix} \mathbf{q}_m \\ \mathbf{q}_e \end{Bmatrix}^{\mathrm{T}} \mathbf{k}^e \begin{Bmatrix} \mathbf{q}_m \\ \mathbf{q}_e \end{Bmatrix} - \langle \bar{\mathbf{b}}^{\mathrm{T}} \mathbf{N}_m \rangle \mathbf{q}_m - P_s^e, \tag{21a}$$

$$\mathbf{k}^e = \begin{bmatrix} \langle \mathbf{B}_m^{\mathrm{T}} \mathbf{c}_E \mathbf{B}_m \rangle & \langle \mathbf{B}_m^{\mathrm{T}} \mathbf{e}^{\mathrm{T}} \mathbf{B}_e \rangle \\ \langle \mathbf{B}_e^{\mathrm{T}} \mathbf{e} \mathbf{B}_m \rangle & -\langle \mathbf{B}_e^{\mathrm{T}} \boldsymbol{\varepsilon}_\gamma \mathbf{B}_e \rangle \end{bmatrix} \text{ is the element matrix.} \tag{21b}$$

2. *Finite element formulation using* $\Pi_D = \sum_e \Pi_D^e$—the elementwise version of Π_D is

$$\Pi_D^e = \int_{\Omega^e} \left[\frac{1}{2} \begin{Bmatrix} \mathscr{D}_m \mathbf{u} \\ \mathbf{D} \end{Bmatrix}^{\mathrm{T}} \begin{bmatrix} \mathbf{c}_D & -\mathbf{h}^{\mathrm{T}} \\ -\mathbf{h} & \mathbf{f}_\gamma \end{bmatrix} \begin{Bmatrix} \mathscr{D}_m \mathbf{u} \\ \mathbf{D} \end{Bmatrix} + \mathbf{D}^{\mathrm{T}} \mathscr{D}_e \phi - \bar{\mathbf{b}}^{\mathrm{T}} \mathbf{u} \right] \mathrm{d}v - P_S^e. \tag{22}$$

With equations (18) and (19) invoked

$$\Pi_D^e = \frac{1}{2} \begin{Bmatrix} \mathbf{q}_m \\ \boldsymbol{\beta}_e \end{Bmatrix}^{\mathrm{T}} \begin{bmatrix} \langle \mathbf{B}_m^{\mathrm{T}} \mathbf{c}_D \mathbf{B}_m \rangle & -\langle \mathbf{B}_m^{\mathrm{T}} \mathbf{h}^{\mathrm{T}} \mathbf{P}_e \rangle \\ -\langle \mathbf{P}_e^{\mathrm{T}} \mathbf{h} \mathbf{B}_m \rangle & \langle \mathbf{P}_e^{\mathrm{T}} \mathbf{f}_\gamma \mathbf{P}_e \rangle \end{bmatrix} \begin{Bmatrix} \mathbf{q}_m \\ \boldsymbol{\beta}_e \end{Bmatrix} + \boldsymbol{\beta}_e^{\mathrm{T}} \mathbf{P}_e^{\mathrm{T}} \mathbf{B}_e \mathbf{q}_e - \langle \bar{\mathbf{b}}^{\mathrm{T}} \mathbf{N}_m \rangle \mathbf{q}_m - P_S^e. \tag{23}$$

Variation of $\boldsymbol{\beta}_e$ results in

$$\boldsymbol{\beta}_e = \langle \mathbf{P}_e^{\mathrm{T}} \mathbf{f}_\gamma \mathbf{P}_e \rangle^{-1} [\langle \mathbf{P}_e^{\mathrm{T}} \mathbf{h} \mathbf{B}_m \rangle - \langle \mathbf{P}_e^{\mathrm{T}} \mathbf{B}_e \rangle] \begin{Bmatrix} \mathbf{q}_m \\ \mathbf{q}_e \end{Bmatrix} \tag{24}$$

with which

$$\Pi_D^e = \frac{1}{2} \begin{Bmatrix} \mathbf{q}_m \\ \mathbf{q}_e \end{Bmatrix}^{\mathrm{T}} \mathbf{k}_D^e \begin{Bmatrix} \mathbf{q}_m \\ \mathbf{q}_e \end{Bmatrix} - \langle \bar{\mathbf{b}}^{\mathrm{T}} \mathbf{N}_m \rangle \mathbf{q}_m - P_s^e, \tag{25a}$$

$$\mathbf{k}_D^e = \begin{bmatrix} \langle \mathbf{B}_m^{\mathrm{T}} \mathbf{c}_D \mathbf{B}_m \rangle & \mathbf{0} \\ \mathbf{0} & \mathbf{0} \end{bmatrix} - \begin{bmatrix} \langle \mathbf{P}_e^{\mathrm{T}} \mathbf{h} \mathbf{B}_m \rangle^{\mathrm{T}} \\ -\langle \mathbf{P}_e^{\mathrm{T}} \mathbf{B}_e \rangle^{\mathrm{T}} \end{bmatrix} \langle \mathbf{P}_e^{\mathrm{T}} \mathbf{f}_\gamma \mathbf{P}_e \rangle^{-1} [\langle \mathbf{P}_e^{\mathrm{T}} \mathbf{h} \mathbf{B}_m \rangle - \langle \mathbf{P}_e^{\mathrm{T}} \mathbf{B}_e \rangle]. \tag{25b}$$

3. *Finite element formulation using* $\Pi_\tau = \sum_e \Pi_\tau^e$—the elementwise version of Π_τ is

$$\Pi_\tau^e = \int_{\Omega^e} \left(\frac{-1}{2} \begin{Bmatrix} \boldsymbol{\tau} \\ \mathscr{D}_e \phi \end{Bmatrix}^{\mathrm{T}} \begin{bmatrix} \mathbf{s}_E & -\mathbf{d}^{\mathrm{T}} \\ -\mathbf{d} & \boldsymbol{\varepsilon}_\tau \end{bmatrix} \begin{Bmatrix} \boldsymbol{\tau} \\ \mathscr{D}_e \phi \end{Bmatrix} + \boldsymbol{\tau}^{\mathrm{T}} \mathscr{D}_m \mathbf{u} - \bar{\mathbf{b}}^{\mathrm{T}} \mathbf{u} \right) \mathrm{d}v - P_S^e. \quad (26)$$

With equations (18) and (19) invoked

$$\Pi_\tau^e = \frac{-1}{2} \begin{Bmatrix} \boldsymbol{\beta}_m \\ \mathbf{q}_e \end{Bmatrix}^{\mathrm{T}} \begin{bmatrix} \langle \mathbf{P}_m^{\mathrm{T}} \mathbf{s}_E \mathbf{P}_m \rangle & -\langle \mathbf{P}_m^{\mathrm{T}} \mathbf{d}^{\mathrm{T}} \mathbf{B}_e \rangle \\ -\langle \mathbf{B}_e^{\mathrm{T}} \mathbf{d} \mathbf{P}_m \rangle & \langle \mathbf{B}_e^{\mathrm{T}} \boldsymbol{\varepsilon}_t \mathrm{B}_e \rangle \end{bmatrix} \begin{Bmatrix} \boldsymbol{\beta}_m \\ \mathbf{q}_e \end{Bmatrix} + \boldsymbol{\beta}_m^{\mathrm{T}} \langle \mathbf{P}_m^{\mathrm{T}} \mathbf{B}_m \rangle \mathbf{q}_m - \langle \bar{\mathbf{b}}^{\mathrm{T}} \mathbf{N}_m \rangle \mathbf{q}_m - P_s^e. \quad (27)$$

Variation of $\boldsymbol{\beta}_m$ results in

$$\boldsymbol{\beta}_m = \langle \mathbf{P}_m^{\mathrm{T}} \mathbf{s}_E \mathbf{P}_m \rangle^{-1} [\langle \mathbf{P}_m^{\mathrm{T}} \mathbf{B}_m \rangle \ \langle \mathbf{P}_m^{\mathrm{T}} \mathbf{d}^{\mathrm{T}} \mathbf{B}_e \rangle] \begin{Bmatrix} \mathbf{q}_m \\ \mathbf{q}_e \end{Bmatrix} \quad (28)$$

with which

$$\Pi_\tau^e = \frac{1}{2} \begin{Bmatrix} \mathbf{q}_m \\ \mathbf{q}_e \end{Bmatrix}^{\mathrm{T}} \mathbf{k}_\tau^e \begin{Bmatrix} \mathbf{q}_m \\ \mathbf{q}_e \end{Bmatrix} - \langle \bar{\mathbf{b}}^{\mathrm{T}} \mathbf{N}_m \rangle \mathbf{q}_m - P_S^e, \quad (29a)$$

$$\mathbf{k}_\tau^e = \begin{bmatrix} \langle \mathbf{P}_m^{\mathrm{T}} \mathbf{B}_m \rangle^{\mathrm{T}} \\ \langle \mathbf{P}_m^{\mathrm{T}} \mathbf{d}^{\mathrm{T}} \mathbf{B}_e \rangle^{\mathrm{T}} \end{bmatrix} \langle \mathbf{P}_m^{\mathrm{T}} \mathbf{s}_E \mathbf{P}_m \rangle^{-1} [\langle \mathbf{P}_m^{\mathrm{T}} \mathbf{B}_m \rangle \ \langle \mathbf{P}_m^{\mathrm{T}} \mathbf{d}^{\mathrm{T}} \mathbf{B}_e \rangle] - \begin{bmatrix} \mathbf{0} & \mathbf{0} \\ \mathbf{0} & \langle \mathbf{B}_e^{\mathrm{T}} \boldsymbol{\varepsilon}_\tau \mathrm{B}_e \rangle \end{bmatrix}. \quad (29b)$$

4. *Finite element formulation using* $\Pi_{\tau D} = \sum_e \Pi_{\tau D}^e$—the elementwise version of $\Pi_{\tau D}$ is

$$\Pi_{\tau D}^e = \int_{\Omega^e} \left(\frac{-1}{2} \begin{Bmatrix} \boldsymbol{\tau} \\ \mathbf{D} \end{Bmatrix}^{\mathrm{T}} \begin{bmatrix} \mathbf{S}_D & \mathbf{g}^{\mathrm{T}} \\ \mathbf{g} & -\mathbf{f}_\tau \end{bmatrix} \begin{Bmatrix} \boldsymbol{\tau} \\ \mathbf{D} \end{Bmatrix} + \begin{Bmatrix} \boldsymbol{\tau} \\ \mathbf{D} \end{Bmatrix}^{\mathrm{T}} \begin{Bmatrix} \mathscr{D}_m \mathbf{u} \\ \mathscr{D}_e \phi \end{Bmatrix} - \bar{\mathbf{b}}^{\mathrm{T}} \mathbf{u} \right) \mathrm{d}v - P_S^e. \quad (30)$$

with equations (18) and (19) invoked

$$\Pi_{\tau D}^e = \frac{-1}{2} \begin{Bmatrix} \boldsymbol{\beta}_m \\ \boldsymbol{\beta}_e \end{Bmatrix}^{\mathrm{T}} \begin{bmatrix} \langle \mathbf{P}_m^{\mathrm{T}} \mathbf{S}_D \mathbf{P}_m \rangle & \langle \mathbf{P}_m^{\mathrm{T}} \mathbf{g}^{\mathrm{T}} \mathbf{P}_e \rangle \\ \langle \mathbf{P}_e^{\mathrm{T}} \mathbf{g} \mathbf{P}_m \rangle & -\langle \mathbf{P}_e^{\mathrm{T}} \mathbf{f}_e \mathbf{P}_e \rangle \end{bmatrix} \begin{Bmatrix} \boldsymbol{\beta}_m \\ \boldsymbol{\beta}_e \end{Bmatrix} + \begin{Bmatrix} \boldsymbol{\beta}_m \\ \boldsymbol{\beta}_e \end{Bmatrix}^{\mathrm{T}} \times \begin{bmatrix} \langle \mathbf{P}_m^{\mathrm{T}} \mathbf{B}_m \rangle & \mathbf{0} \\ \mathbf{0} & -\langle \mathbf{P}_e^{\mathrm{T}} \mathbf{B}_e \rangle \end{bmatrix} \begin{Bmatrix} \mathbf{q}_m \\ \mathbf{q}_e \end{Bmatrix}_m - \langle \bar{\mathbf{b}}^{\mathrm{T}} \mathbf{N}_m \rangle \mathbf{q}_m - \mathbf{P}_S^e. \quad (31)$$

Variation of $\boldsymbol{\beta}_m$ and $\boldsymbol{\beta}_e$ results in

$$\begin{Bmatrix} \boldsymbol{\beta}_m \\ \boldsymbol{\beta}_e \end{Bmatrix} = \begin{bmatrix} \langle \mathbf{P}_m^{\mathrm{T}} \mathbf{S}_D \mathbf{P}_m \rangle & \langle \mathbf{P}_m^{\mathrm{T}} \mathbf{g}^{\mathrm{T}} \mathbf{P}_e \rangle \\ \langle \mathbf{P}_e^{\mathrm{T}} \mathbf{g} \mathbf{P}_m \rangle & -\langle \mathbf{P}_e^{\mathrm{T}} \mathbf{f}_\sigma \mathbf{P}_e \rangle \end{bmatrix}^{-1} \begin{bmatrix} \langle \mathbf{P}_m^{\mathrm{T}} \mathbf{B}_m \rangle & \mathbf{0} \\ \mathbf{0} & \langle \mathbf{P}_e^{\mathrm{T}} \mathbf{B}_e \rangle \end{bmatrix} \begin{Bmatrix} \mathbf{q}_m \\ \mathbf{q}_e \end{Bmatrix} \quad (32)$$

with which

$$\Pi^e_{\tau D} = \frac{1}{2}\begin{Bmatrix}\mathbf{q}_m\\ \mathbf{q}_e\end{Bmatrix}^{\mathrm{T}} \mathbf{k}^e_{\tau D}\begin{Bmatrix}\mathbf{q}_m\\ \mathbf{q}_e\end{Bmatrix} - \langle \bar{\mathbf{b}}^{\mathrm{T}}\mathbf{N}_m\rangle \mathbf{q}_m - P^e_S, \tag{33a}$$

$$\mathbf{k}^e_{\tau D} = \begin{bmatrix}\langle \mathbf{P}_m^{\mathrm{T}}\mathbf{B}_m\rangle & \mathbf{0}\\ \mathbf{0} & \langle \mathbf{P}_e^{\mathrm{T}}\mathbf{B}_e\rangle\end{bmatrix}\begin{bmatrix}\langle \mathbf{P}_m^{\mathrm{T}}\mathbf{S}_D\mathbf{P}_m\rangle & \langle \mathbf{P}_m^{\mathrm{T}}\mathbf{g}^{\mathrm{T}}\mathbf{P}_e\rangle\\ \langle \mathbf{P}_e^{\mathrm{T}}\mathbf{g}\mathbf{P}_m\rangle & -\langle \mathbf{P}_e^{\mathrm{T}}\mathbf{f}_\sigma\mathbf{P}_e\rangle\end{bmatrix}^{-1}\begin{bmatrix}\langle \mathbf{P}_m^{\mathrm{T}}\mathbf{B}_m\rangle & \mathbf{0}\\ \mathbf{0} & \langle \mathbf{P}_e^{\mathrm{T}}\mathbf{B}_e\rangle\end{bmatrix}. \tag{33b}$$

7. DETERMINATION OF EIGENFREQUENCIES

In eigenfrequency analysis, the surface loads vanish and the inertial force can be incorporated as the body force, i.e., $\bar{\mathbf{b}} = -\rho\ddot{\mathbf{u}}$. Similar to the conventional eigenfrequency analysis, we assume

$$\mathbf{u} = \tilde{\mathbf{u}}\mathrm{e}^{\mathrm{i}\theta t}, \quad \phi = \tilde{\phi}\mathrm{e}^{\mathrm{i}\theta t}, \quad \boldsymbol{\tau} = \tilde{\boldsymbol{\tau}}\mathrm{e}^{\mathrm{i}\theta t}, \quad \mathbf{D} = \tilde{\mathbf{D}}\mathrm{e}^{\mathrm{i}\theta t} \quad \text{and thus} \quad \ddot{\mathbf{u}} = -\theta^2\mathbf{u}, \tag{34}$$

where quantities with tilde denote their amplitudes, t is time and θ is the eigenfrequency. In finite element formulation and within each element,

$$\mathbf{u} = \mathbf{N}_m\tilde{\mathbf{q}}_m\mathrm{e}^{\mathrm{i}\theta t}, \quad \phi = \mathbf{N}_e\tilde{\mathbf{q}}_e\mathrm{e}^{\mathrm{i}\theta t}, \quad \boldsymbol{\tau} = \mathbf{P}_m\tilde{\boldsymbol{\beta}}_m\mathrm{e}^{\mathrm{i}\theta t}, \quad \mathbf{D} = \mathbf{P}_e\tilde{\boldsymbol{\beta}}_e\mathrm{e}^{\mathrm{i}\theta t}. \tag{35}$$

It is trivial to show that the elementwise variational functionals in equations (20), (22), (26) and (30) will take the following form:

$$\Pi^e = \mathrm{e}^{2\mathrm{i}\theta t}\sum_e \frac{1}{2}\begin{Bmatrix}\tilde{\mathbf{q}}_m\\ \tilde{\mathbf{q}}_e\end{Bmatrix}^{\mathrm{T}}(\mathbf{k}^e + \theta^2\langle\rho\mathbf{N}_m^{\mathrm{T}}\mathbf{N}_m\rangle)\begin{Bmatrix}\tilde{\mathbf{q}}_m\\ \tilde{\mathbf{q}}_e\end{Bmatrix}, \tag{36}$$

which is stationary w.r.t. the nodal amplitude d.o.f.s. A standard eigenvalue problem results.

8. INTERPOLATION AND SHAPE FUNCTIONS

In this section, a number of three-dimensional eight-node piezoelectric elements will be developed. For the eight-node element as depicted in Figure 2, the interpolation function for the ith node is

$$N_t = \tfrac{1}{8}(1 + \xi_i\xi)(1 + \eta_i\eta)(1 + \zeta_i\zeta), \tag{37}$$

where ξ, η and $\zeta \in [-1, +1]$ are the natural co-ordinates. Here, quantities with subscripts denote their nodal counterparts. The co-ordinates, displacement and

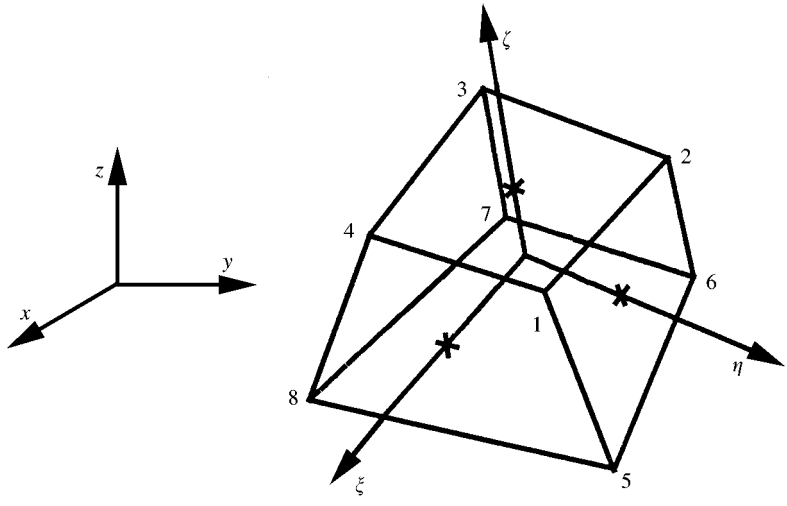

Figure 2. An eight-node hexahedral element and its node numbering sequence.

electric potential are interpolated as

$$x=\sum_{i=1}^{8} N_i x_i, \quad y=\sum_{i=1}^{8} N_i y_i, \quad z=\sum_{i=1}^{8} N_i z_i, \quad \phi=[N_1, \ldots, N_8]\{\phi_1, \ldots, \phi_8\}^{\mathrm{T}}=\mathbf{N}_e\mathbf{q}_e, \tag{38a}$$

$$\mathbf{u}=[N_1\mathbf{I}_3, \ldots, N_8\mathbf{I}_3]\{u_1, v_1, w_1, \ldots, u_8, v_8, w_8\}^{\mathrm{T}}=\mathbf{N}_m\mathbf{q}_m, \tag{38b}$$

where $\mathbf{I}_i$ is the ith order identity matrix. The following geometric parameters are defined for subsequent use

$$\mathbf{T}_e=\begin{bmatrix} a_1 & b_1 & c_1 \\ a_2 & b_2 & c_2 \\ a_3 & b_3 & c_3 \end{bmatrix}=\begin{bmatrix} \partial x/\partial\xi & \partial y/\partial\xi & \partial z/\partial\xi \\ \partial x/\partial\eta & \partial y/\partial\eta & \partial z/\partial\eta \\ \partial x/\partial\zeta & \partial y/\partial\zeta & \partial z/\partial\zeta \end{bmatrix}\Bigg|_{\xi=\eta=\zeta=0}, \tag{39a}$$

which can be worked out to be

$$\mathbf{T}_e=\begin{bmatrix} a_1 & b_1 & c_1 \\ a_2 & b_2 & c_2 \\ a_3 & b_3 & c_3 \end{bmatrix}=\frac{1}{8}\begin{bmatrix} -1 & +1 & +1 & -1 & -1 & +1 & +1 & -1 \\ -1 & -1 & +1 & +1 & -1 & -1 & +1 & +1 \\ -1 & -1 & -1 & -1 & +1 & +1 & +1 & +1 \end{bmatrix}$$

$$\times\begin{Bmatrix} x_1 & y_1 & z_1 \\ \vdots & \vdots & \vdots \\ x_8 & y_8 & z_8 \end{Bmatrix}. \tag{39b}$$

It has been well-known that the element based solely on the above displacement interpolation is too stiff, susceptible to mesh distortion and aspect ratio. Ha *et al.* [16] and Tzou [17] have supplemented the interpolated displacement with Wilson's incompatible modes [24, 25]:

$$\mathbf{u} = \mathbf{N}_m \mathbf{q}_m + [(1-\xi^2)\mathbf{I}_3, (1-\eta^2)\mathbf{I}_3, (1-\zeta^2)\mathbf{I}_3] \begin{Bmatrix} \lambda_1 \\ \vdots \\ \lambda_9 \end{Bmatrix}. \tag{40}$$

It should be remarked that a modified strain–displacement operator suggested by Taylor *et al.* must be used [24]. Otherwise, the resulting element will fail the patch test. In finite element implementation, λ_i's are internal displacement d.o.f.s not shared by the adjacent elements. Hence, they can be condensed in the element level.

For the assumed stress, the one in Pian's element [34, 37] is employed. The element contains 18 stress modes which are minimal for securing the proper element rank. The stress in the element can be expressed as

$$\boldsymbol{\tau} = \mathbf{P}_m \boldsymbol{\beta}_m = [\mathbf{I}_6 \;\; \mathbf{T}_m \mathbf{P}_m] \begin{Bmatrix} \boldsymbol{\beta}_{mc} \\ \boldsymbol{\beta}_{mh} \end{Bmatrix}, \tag{41a}$$

in which

$$P_{mh} = \begin{bmatrix} 0 & 0 & 0 & \eta & 0 & 0 & \zeta & 0 & 0 & \eta\zeta & 0 & 0 \\ \xi & 0 & 0 & 0 & 0 & 0 & 0 & \zeta & 0 & 0 & \zeta\xi & 0 \\ 0 & \xi & 0 & 0 & \eta & 0 & 0 & 0 & 0 & 0 & 0 & \xi\eta \\ 0 & 0 & 0 & 0 & 0 & 0 & 0 & 0 & \zeta & 0 & 0 & 0 \\ 0 & 0 & \xi & 0 & 0 & 0 & 0 & 0 & 0 & 0 & 0 & 0 \\ 0 & 0 & 0 & 0 & 0 & \eta & 0 & 0 & 0 & 0 & 0 & 0 \end{bmatrix}, \tag{41b}$$

is the higher order contravariant stress shape function matrix and

$$\mathbf{T}_m = \begin{bmatrix} a_1^2 & a_2^2 & a_3^2 & 2a_1a_2 & 2a_2a_3 & 2a_3a_1 \\ b_1^2 & b_2^2 & b_3^2 & 2b_1b_2 & 2b_2b_3 & 2b_3b_1 \\ c_1^2 & c_2^2 & c_3^2 & 2c_1c_2 & 2c_2c_3 & 2c_3c_1 \\ a_1b_1 & a_2b_2 & a_3b_3 & a_1b_2+a_2b_1 & a_2b_3+a_3b_2 & a_3b_1+a_1b_3 \\ b_1c_1 & b_2c_2 & b_3c_3 & b_1c_2+b_2c_1 & b_2c_3+b_3c_2 & b_3c_1+b_1c_3 \\ c_1a_1 & c_2a_2 & c_3a_3 & c_1a_2+c_2a_1 & c_2a_3+c_3a_2 & c_3a_1+c_1a_3 \end{bmatrix}, \tag{41c}$$

is the transformation matrix evaluated at the element origin for the contravariant and Cartesian stresses. It can be proven that the above stress is in strict homogenous equilibrium when the element Jacobian determinant is a constant.

For the electric displacement, the minimum number of assumed modes for securing the proper element rank is seven. To devise the electric displacement modes, a $2 \times 2 \times 2$ element with its natural and Cartesian co-ordinate axes parallel is considered. The interpolated electric potential can be expressed as

$$\phi = [1 \;\; \xi \;\; \eta \;\; \zeta \;\; \xi\eta \;\; \eta\zeta \;\; \zeta\xi \;\; \xi\eta\zeta] \begin{Bmatrix} \psi_1 \\ \vdots \\ \psi_8 \end{Bmatrix}, \tag{42}$$

where ψ_is are linear combinations of the element nodal electrical potential. The derived electric field is

$$\mathbf{E} = \begin{Bmatrix} E_\xi \\ E_\xi \\ E_\xi \end{Bmatrix} = -\begin{Bmatrix} \partial/\partial\xi \\ \partial/\partial\eta \\ \partial/\partial\zeta \end{Bmatrix} \phi = -\begin{bmatrix} 0 & 1 & 0 & 0 & \eta & 0 & \zeta & \eta\zeta \\ 0 & 0 & 1 & 0 & \xi & \zeta & 0 & \zeta\xi \\ 0 & 0 & 0 & 1 & 0 & \eta & \xi & \xi\eta \end{bmatrix} \begin{Bmatrix} \psi_1 \\ \vdots \\ \psi_8 \end{Bmatrix}. \tag{43}$$

Recalling that $-\mathbf{E}$ and $\mathbf{D}$ are energy conjugates, the four non-constant or higher order electric field can be suppressed or matched by the following contravariant electric displacement modes:

$$\begin{Bmatrix} D_\xi \\ D_\eta \\ D_\zeta \end{Bmatrix} = \mathbf{P}_{eh}\boldsymbol{\beta}_{eh} = \begin{bmatrix} \eta & 0 & \zeta & \eta\zeta \\ \xi & \zeta & 0 & \zeta\xi \\ 0 & \eta & \xi & \xi\eta \end{bmatrix} \boldsymbol{\beta}_{eh}. \tag{44}$$

For a generic element, the assumed higher order Cartesian electric displacement can be transformed from $\mathbf{P}_{eh}\boldsymbol{\beta}_{eh}$. With the constant electric displacement augmented, the complete assumed electric displacement is

$$\mathbf{D} = \mathbf{P}_e\boldsymbol{\beta}_e = [\mathbf{I}_3 \;\; \mathbf{T}_e\mathbf{P}_{eh}] \begin{Bmatrix} \boldsymbol{\beta}_{ec} \\ \boldsymbol{\beta}_{eh} \end{Bmatrix}, \tag{45}$$

where $\mathbf{T}_e$ as defined in equation (39) is the transformation matrix for the contravariant and Cartesian electric displacements evaluated at the element origin. It can be shown that the above assumed electric displacement satisfies the charge conservation condition when the element Jacobian determinant is a constant.

9. NUMERICAL EXAMPLES

In this section, a number of benchmark problems are examined. Predictions of the following elements are included for comparisons:

H8—the irreducible element based on Π, the displacement and electric potential are given in equation (38).

H8I—the irreducible incompatible element based on Π, the electric potential and displacement are given in equation (38) and (40) respectively.

H8D—the hybrid element based on Π_D, electric displacement is given in equation (45) whereas displacement and electric potential are given in equation (38).

H8DI—the hybrid incompatible element based on Π_D, the electric potential, displacement and electric displacement are given in equations (38), (40) and (45) respectively.

H8S—the hybrid element based on Π_τ, stress is given in equation (41) whereas displacement and electric potential are given in equation (38).

H8DS—the hybrid element based on $\Pi_{D\tau}$, the stress is given in equation (41), electric displacement is given in equation (45) whereas displacement and electric potential are given in equation (38).

In the element abbreviations, "H", "8", "I", "D", "S" stand for hexahedron, eight-node, incompatible displacement, assumed electric displacement and assumed stress respectively. All elements are evaluated by the second order Gaussian rule which is sufficient to secure the proper element rank.

9.1. BIMORPH BEAM

The bimorph beam is presented in the text of Tzou [17]. It consists of two identical PVDF uni-axial layers with opposite polarities, and hence will bend when an electric field is applied in the transverse direction. Properties of PVDF are extracted from reference [17] and listed in Table 1. The bimorph is here modelled by eight elements at four elements per layer as depicted in Figure 3. With a unit voltage applied across the thickness, the free end deflection and normalized bending stress at the Gaussian point "A" closest to the top face are computed. The effect of mesh distortion on element accuracy is examined by varying "e". The results are shown in Figures 4 and 5. It can be seen that H8S/H8DS are better than H8I/H8DI whereas H8/H8D are extremely poor even at $e = 0$. All these elements are very sensitive to mesh distortion as a result of shear locking. Using a selective scaling technique which was developed for alleviated shear locking in hybrid stress solid elements [37], H8S/H8DS yield much better predictions as denoted by H8S*/H8DS* in the figures. H8DS* is marginally more accurate than H8S*.

9.2. CANTILEVER BEAM

The problem depicted in Figure 6 was considered by Saravanos and Heyliger [45]. The cantilever consists of a thick layer of uni-directional graphite/epoxy and a thin layer of PZT-4 piezoceramic adhered together. The figure runs along the longitudinal direction of the beam. The material properties are listed in Table 1. The beam is modelled with a total of 5×8 elements. The piezoelectric layer is modelled by a layer of eight elements, whereas the graphite/epoxy is modelled by four layers of eight elements. A 12·5 kV potential difference is applied across the piezoelectric layer. The computed deflection curve is shown in Figure 7. In obtaining the prediction from ABAQUS [46] for comparison, the cantilever is

TABLE 1

Material properties

	T300/934 Gr/Epoxy	PZT-4	PVDF	AI
Elastic properties (in $\mathbf{c}_E$)				
E_{11} (GPa)	132·8	83·0	2·0	68·9
E_{22} (GPa)	10·76	81·3	2·0	68·9
E_{33} (GPa)	10·96	66·0	2·0	68·9
$G_{12} = G_{13}$(GPa)	5·65	31·0		
G_{23} (GPa)	3·61	25·6		
$v_{12} = v_{13}$	0·24	0·31	0·29	0·25
v_{23}	0·49	0·43	0·29	0·25
Piezoelectric coefficients (in matrix **d** or **e**)				
$d_{31} = d_{32}$ (10^{-12} m/V)		−122		
d_{33} (10^{-12} m/V		285		
e_{31} (C/m^2)			0·046	
Electric permittivity coefficients (in matrix $\mathbf{e}_\gamma$)				
$\varepsilon_{11} = \varepsilon_{22}$ (10^{-8} F/m)		1·3054	0·01062	
ε_{33} (10^{-8} F/m)		1·1505	0·01062	
Mass density (kg/m^3)	1578	7600	1800	2769

modelled by a total of 3×16 20-node hexahedral piezoelectric elements with one element layer for PZT-4 and two element layers for graphite/epoxy. As ABAQUS does not have an eight-node piezoelectric element, the 20-node hexahedral element with designation C3D20E is selected [46]. The element is irreducible and fully integrated by the third order quadrature. In Figure 7, the results of Koko *et al.* [20] were calculated by 2×8 elements 20-node composite elements. Predictions of all the eight-node elements are in between those of Koko *et al.* [20] and ABAQUS. As the beam is quite thick, even H8/H8D can yield accurate results.

With graphite/epoxy replaced by aluminium (see Table 1 for material properties), eigenfrequencies of the structure is computed. Two circuit arrangements are considered. The first is an open circuit in which the bottom surface of the PZT-4 layer is grounded. The second is a closed circuit in which the top and bottom surfaces of the PZT-4 layer are both grounded. The ten lowest eigenfrequencies are presented in Tables 2 and 3. H8/H8D are stiffest as the predicted frequencies are much higher than that by H8I/H8DI, and H8S/H8DS. The tables also list the predictions given by Koko *et al.* [20] and evaluated by ABAQUS. All the results are based on the same meshes described in the previous paragraph.

It can be seen in Tables 2 and 3 that the first six frequencies predicted by H8I/H8DI and H8S/H8DS are in good agreement with those of Koko *et al.* and ABAQUS. The differences are in the order of 0·5%. When the beam is modelled by

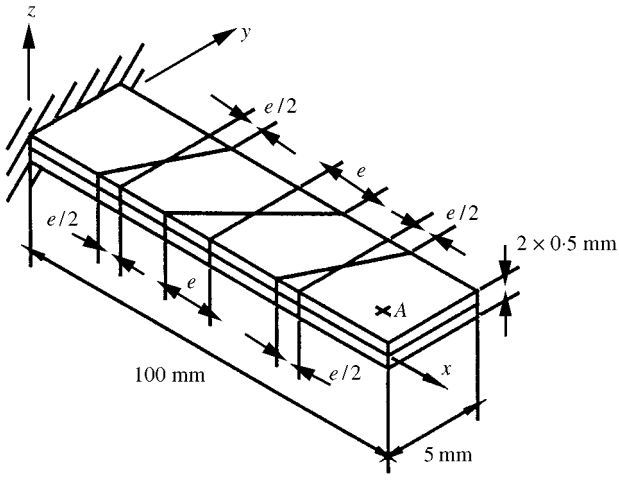

Figure 3. A bimorph cantilever.

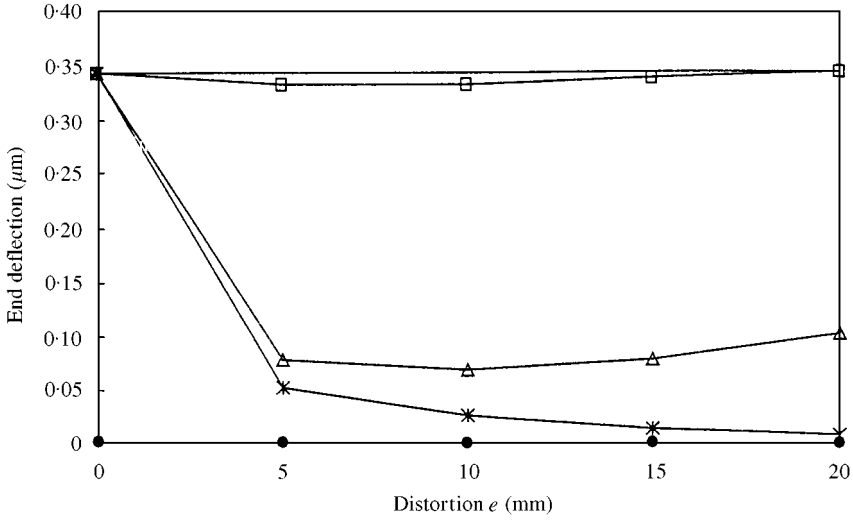

Figure 4. Effect of mesh distortion on the end deflection of the bimorph cantilever in Figure 3; H8S* and H8DS* employ the selective scaling technique [37]: —●— H8, H8D; —∗— HBI, H8D; —△— H8S, H8DS; —□— H8S; H8DS; —— analytical [17].

denser meshes, the difference in the higher order frequencies are reduced. For instance, the seventh and tenth frequencies predicted by 5×16 H8I/H8DI elements are 8803 and 16 095 Hz whereas the same frequencies predicted by the same number of H8S/H8DS elements are 8781 and 16 045 Hz under the open-circuit arrangement. The dynamic predictions of H8S/H8DS are slightly more accurate than those of H8I/H8DI.

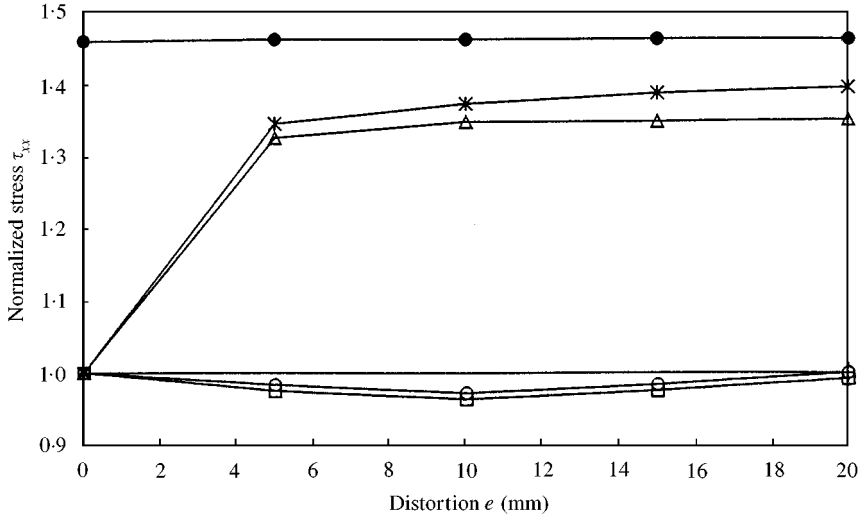

Figure 5. Effect of mesh distortion on the bending stress τ_{xx} in the bimorph cantilever, see Figure 3; H8S* and H8DS* employ the selective scaling technique [37]: —●— H8, H8D; —∗— HBI, H8DI; —△— H8S, H8DS; —□— H8S; —●— H8DS; —— analytical [17].

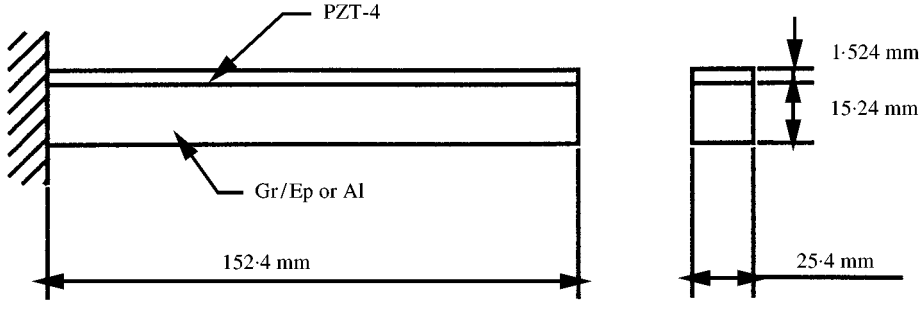

Figure 6. A cantilever with an adhered piezoelectric layer.

9.3. SIMPLY SUPPORTED LAMINATED SQUARE PLATE WITH BONDED PZT-4 LAYERS

The problem portrayed in Figure 8 was first considered by Saravanos and Heyliger [22]. The structure is a simply supported square plate made of T300/934 graphite/epoxy with lay up [0/90/0]. Two layers of the PZT-4 are bonded to the top and bottom surface of the plate. The material properties have been given in Table 1. The length of the plate L is 0·4 m and its total thickness h is 0·008 m. The surfaces of the PZT-4 layers in contact with the graphite/epoxy laminate are grounded. Owing to symmetry, only the lower left hand quadrant of the structure is analyzed. Using one layer of elements for each of the lamina and PZT-layer, $5 \times 4 \times 4$ and $5 \times 8 \times 8$ eight-node elements are employed for an eigenfrequency analysis. For comparison, the problem is also attempted by ABAQUS with $5 \times 8 \times 8$ C3D20E 20-node elements. The ten lowest computed frequencies are listed in Table 4. It can be noted that H8S/H8DS are more accurate than H8I/H8DI, especially for the higher frequencies using the coarse mesh. Again, H8DS are marginally more accurate than H8S.

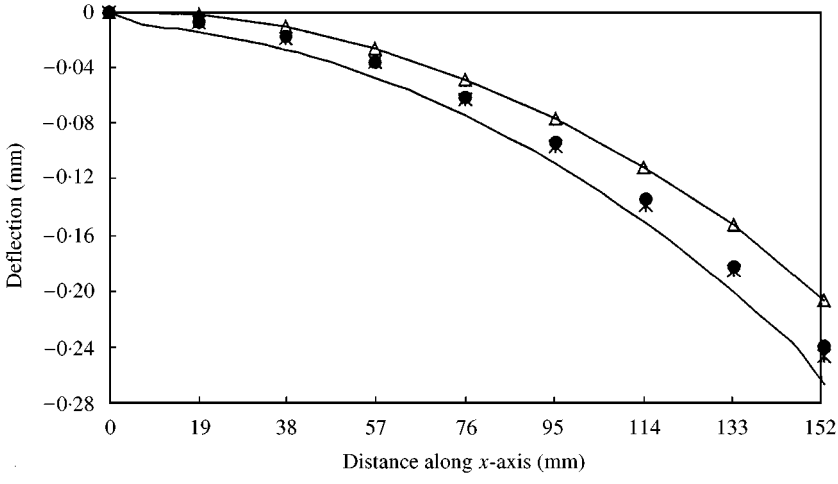

Figure 7. Deflection curve of the cantilever shown in Figure 6 under electric loading: ● H8, H8D; ∗ H8I, H8DI, H8S, H8DS; —△— Koko et al. [20]; —— ABAQUS.

TABLE 2

Eigen frequencies (Hz) *of Al beam with a PZT-4 layers under open circuit, see* Figure 6

Model (no. of elements)	H8I (5 × 8)	H8 (5 × 8)	H8S (5 × 8)	H8ID (5 × 8)	H8D (5 × 8)	H8DS (5 × 8)	Koko [20] (2 × 8)	ABAQUS (3 × 16)
1	562·1	690·0	559·6	562·1	690·0	559·7	556·4	557·8
2	819·5	934·4	815·9	819·6	934·4	815·7	818·3	820·3
3	3447·9	4166·1	3433·3	3448·5	4166·1	3434·5	3307·6	3308·1
4	4305·0	4313·2	4288·0	4305·0	4313·2	4288·0	4323·5	4262·2
5	4807·4	5365·4	4789·4	4807·8	5365·4	4789·3	4651·6	4664·9
6	7771·2	7789·3	7762·4	7771·4	7789·4	7763·1	7721·8	7736·7
7	9503·0	11 243	9455·0	9506·5	11 243	9459·9	8629·0	8603·8
8	12 388	13 030	12 351	12 389	13 030	12 352	11 490	11 485
9	13 252	13 807	13 166	13 253	13 807	13 167	13 047	12 880
10	18 392	21 259	18 280	18 403	21 259	18 293	15 564	15 428

9.4. SIMPLY SUPPORTED LAMINATED SQUARE PLATE WITH BONDED PVDF LAYERS

The problem has been considered by Saravanos *et al.* [13], see Figure 8. It consists of three graphite/epoxy laminae plied at [90/0/90] and two PVDF layers bonded to the top and bottom surfaces. The material properties are listed in Table 5. The total thickness h is 0·01 m and the length to thickness ratio, L/h, is 4. Two load cases are considered. In the first one, a double-sinusoidal electric potential

TABLE 3

Eigen frequencies (Hz) *of Al beam with a PZT-4 layers under closed circuit, see* Figure 6

Model (no. of elements)	H8I (5 × 8)	H8 (5 × 8)	H8S (5 × 8)	H8ID (5 × 8)	H8D (5 × 8)	H8DS (5 × 8)	Koko [20] (2 × 8)	ABAQUS (3 × 16)
1	556·4	683·8	554·3	556·5	683·8	554·5	551·4	551·4
2	816·7	928·4	812·5	816·7	928·4	812·6	817·2	816·4
3	3417	4133	3404	3417	4133	3405	3280	3273
4	4305	4313	4288	4305	4313	4288	4324	4262
5	4794	5337	4773	4794	5337	4774	4646	4646
6	7738	7752	7730	7739	7752	7731	7689	7699
7	9428	11 172	9389	9429	11 172	9392	8573	8522
8	12 364	13 022	12 325	12 364	13 022	12 325	11 479	11 449
9	13 247	13 759	13 158	13 247	13 759	13 160	13 046	12 874
10	18 276	21 160	18 184	18 278	21 160	18 192	15 491	15 297

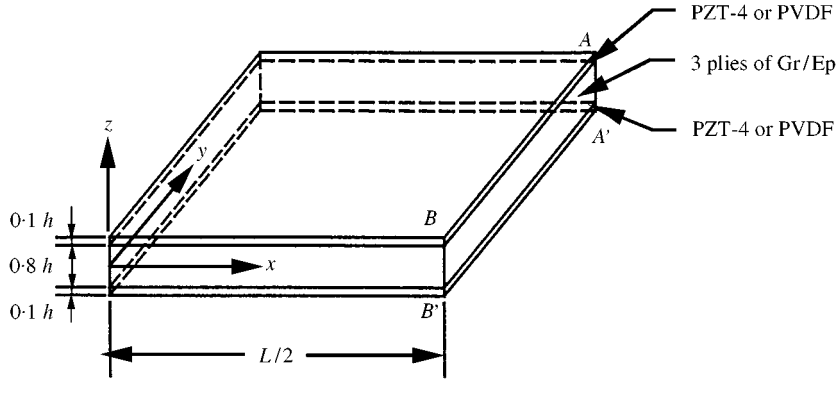

Figure 8. A quadrant of a simply supported three-ply composite plate with two adhered piezoelectric layers. AA′ is the centre of the plate.

given as

$$\bar{\phi} = \sin\frac{\pi x}{L}\sin\frac{\pi y}{L} \tag{46a}$$

is applied to the top surface of the structure whereas the bottom surface and all the vertical edges are grounded. In the second case, a double-sinusoidal load:

$$\bar{t}_z = \sin\frac{\pi x}{L}\sin\frac{\pi y}{L} \tag{46b}$$

TABLE 4

Eigen frequencies (Hz) *of simply supported laminates with PZT-4 layers, see* Figure 8

Mode no.	H8 (4 × 4)	H8I (4 × 4)	H8S (4 × 4)	H8DI (4 × 4)	H8DS (4 × 4)	H8 (8 × 8)	H8I (8 × 8)	H8S (8 × 8)	H8DI (8 × 8)	H8DS (8 × 8)	ABAQUS (8 × 8)
1	439·0	239·2	235·6	239·2	235·5	296·3	232·6	232·4	232·6	232·4	231·4
2	2731·0	1242·0	1205·0	1243·0	1204·0	1553·0	1064·0	1063·0	1065·0	1063·0	1024·0
3	3071·0	1610·0	1578·0	1612·0	1577·0	1852·0	1396·0	1395·0	1396·0	1395·0	1342·0
4	4216·0	2658·0	2317·0	2660·0	2306·0	2625·0	2075·0	2061·0	2076·0	2058·0	1984·0
5	5975·0	4349·0	4212·0	4359·0	4209·0	4264·0	2866·0	2862·0	2868·0	2862·0	2568·0
6	8138·0	5339·0	4930·0	5349·0	4905·0	4956·0	3721·0	3679·0	3724·0	3672·0	3358·0
7	8634·0	5964·0	5209·0	5965·0	5209·0	5019·0	3726·0	3722·0	3729·0	3722·0	3382·0
8	9276·0	6142·0	5680·0	6150·0	5665·0	5512·0	4304·0	4262·0	4307·0	4257·0	3900·0
9	9571·0	6850·0	5964·0	6859·0	5963·0	5935·0	5710·0	5579·0	5714·0	5563·0	4738·0
10	9660·0	8133·0	7388·0	8133·0	7347·0	7139·0	5817·0	5809·0	5824·0	5808·0	5083·0

TABLE 5

Material properties for the piezoelectric laminate

	Graphite/epoxy	PVDF
Elastic coefficients (in matrix $\mathbf{c}_E$)		
c_{11} (GPa)	134·9	238·0
c_{22} (GPa)	14·35	23·6
c_{33} (GPa)	14·35	10·6
c_{12} (GPa)	5·156	3·98
c_{13} (GPa)	5·156	2·19
c_{23} (GPa)	7·133	1·92
c_{44} (GPa)	3·606	2·15
c_{55} (GPa)	5·654	4·40
c_{66} (GPa)	5·654	6·43
Piezoelectric coefficients (in matrix $\mathbf{e}$)		
e_{31} (C/m^2)		−0·13
e_{32} (C/m^2)		−0·14
e_{33} (C/m^2)		−0·28
$e_{25} = e_{16}$ (C/m^2)		−0·01
Permittivity coefficients (in matrix $\mathbf{e}_\gamma$)		
$\varepsilon_{11}/\varepsilon_0$	3·5	12·50
$\varepsilon_{33}/\varepsilon_0 = \varepsilon_{22}/\varepsilon_0$	3·0	11·98
ε_0 (permittivity of free space)	$8{\cdot}854 \times 10^{-12}$ (F/m)	

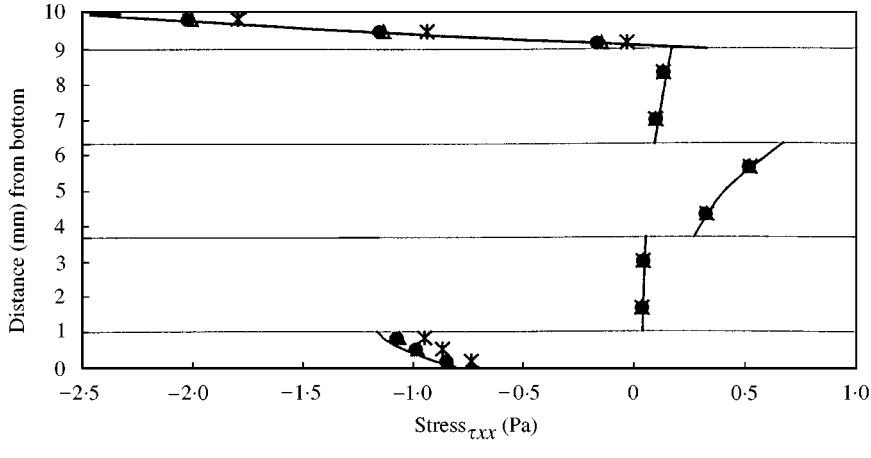

Figure 9. Variation of τ_{xx} along AA′ for the simply supported laminated plate under an applied double-sinusoidal electric potential, see Figure 8: ● H8, H8S; ∗H8DI; △ H8DS; —— Analytical [13].

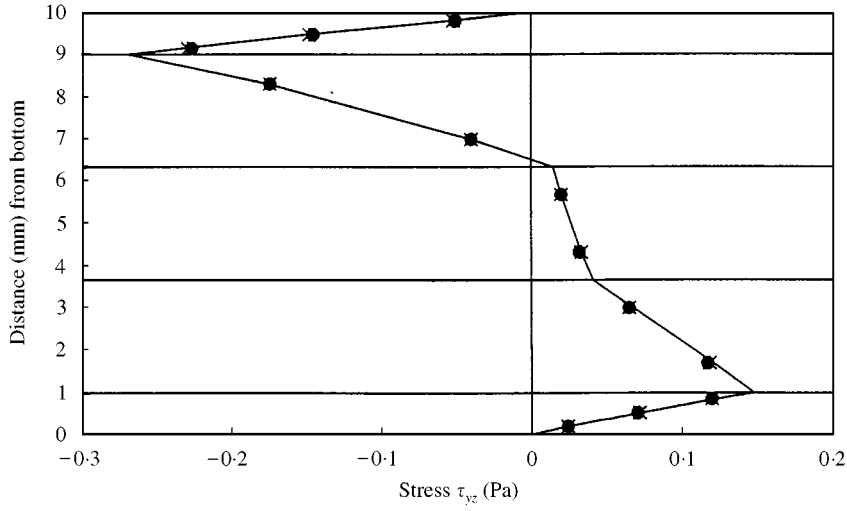

Figure 10. Variation of τ_{yz} along BB′ for the simply supported laminated plate under an applied double-sinusoidal electric potential, see Figure 8: ● H8I, H8S; × H8DI, H8DS; —— analytical [13].

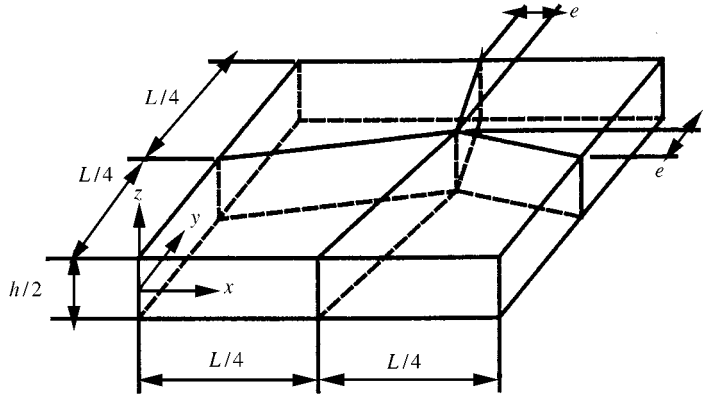

Figure 11. Distorted mesh for the lower left-hand quadrant of the laminated plate, see Figure 8.

is applied to the top surface of the structure whereas all the vertical edges, top and bottom surfaces are grounded. Same as the previous example, only one-quarter of the structure needs to be analyzed. Three element layers are used to model each PVDF layer and two-element layers are used to model each lamina. Hence, a total of 12-element layers are employed in the thickness direction. In constant z-plane, a 4×4 mesh is used. To obtain the stress and electric displacement along AA′ and BB′, their values at the second order quadrature points are extrapolated to the mid-points, which are optimal for linear elements, of the element edges coincident with AA′ and BB′.

Under the double-sinusoidal electric potential, τ_{xx} along AA′ and τ_{yz} along BB′ are plotted in Figures 9 and 10 respectively. H8I/H8DI and H8S/H8DS are all in good agreement with the exact solutions whereas the elements with independently

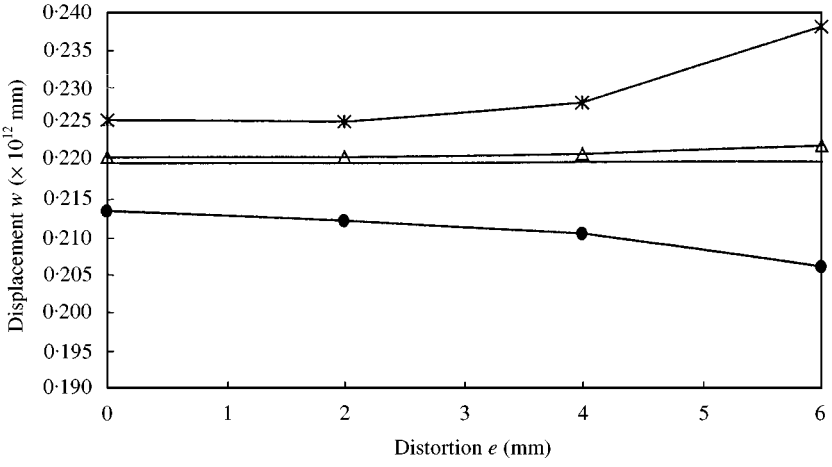

Figure 12. Effect of mesh distortion on the central vertical deflection of the simply supported laminated plate under an applied double-sinusoidal electric potential, see Figure 11: —●— H8I, H8S; —*— H8DI; —△— H8DS; —— analytical [13].

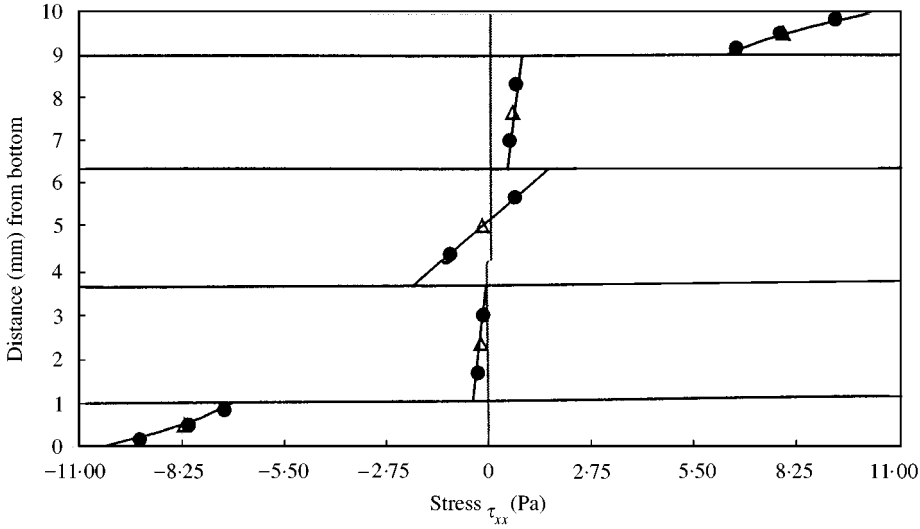

Figure 13. Variation of τ_{xx} along AA′ of the simply supported laminated plate under an applied double-sinusoidal mechanical load, see Figure 11: △ H8S, H8DS, H8I, H8DI (5 layers); ● H8S, H8DS, H8I, H8DI (12 layers); ——analytical [13].

assumed electric displacement, i.e, H8DI and H8DS, are marginally more accurate than their counterparts without assumed electric displacement, i.e. H8I and H8S respectively. The effect of mesh distortion on the central deflection is studied by varying the length "e" in Figure 11, the results of which are shown in Figure 12. It is seen that the assumed electric displacement can improve the element accuracy. The most accurate element is H8DS.

Under the double-sinusoidal mechanical load, τ_{xx} along AA′, shear stress τ_{yz} along BB′, electric potential ϕ along AA′ and electric displacement D_z along AA′ are plotted in Figures 13–16. In Figures 13 and 14, the predictions using five

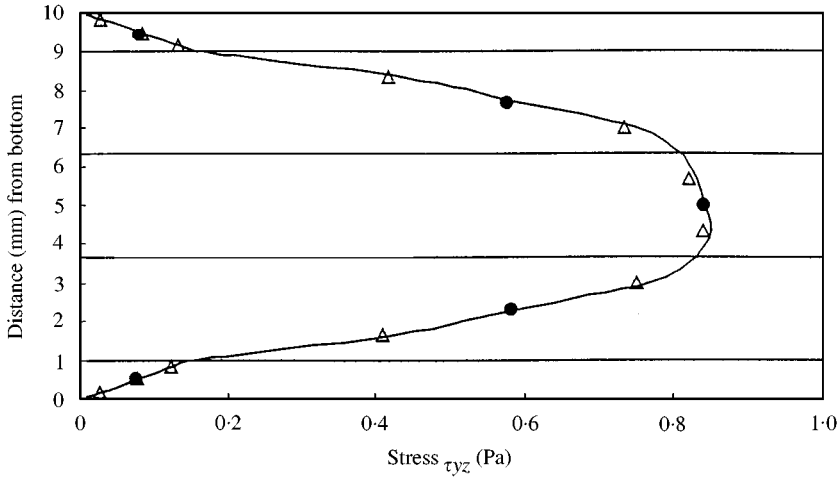

Figure 14. Variation of τ_{yz} along BB′ of the simply supported laminated plate under an applied double-sinusoidal mechanical load, see Figure 8: ● H8I, H8DI, H8S, H8DS (5 layers); △ H8I, H8DI, H8S, H8DS (12 (layers); —— analytical [13].

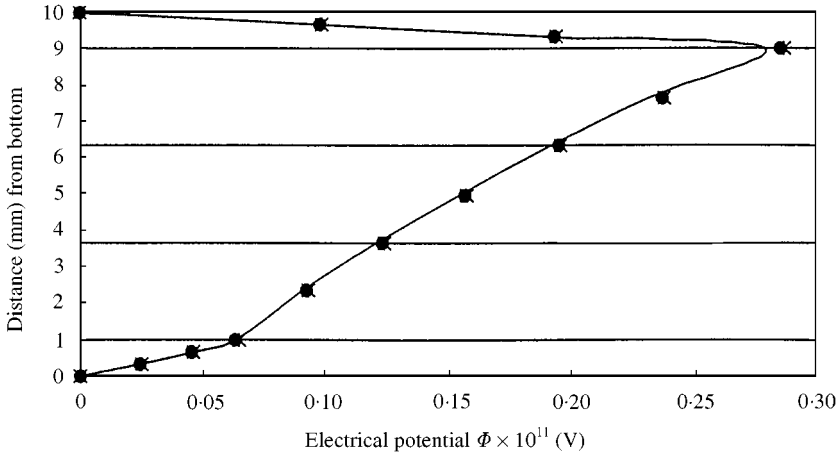

Figure 15. Variation of electric potential along AA′ of the simply supported laminated plate under an applied double-sinusoidal mechanical load, see Figure 8: ● H8I, H8S; ∗ H8DI, H8DS; —— analytical [13].

element layers (one for each of the PVDF layer and graphite/epoxy lamina) are also obtained. All elements yield accurate τ_{xx}, τ_{yz} and ϕ. For D_z shown in Figure 16, all elements yield accurate results in the graphite/epoxy laminate. The ones with assumed electric displacements are the better performers in the PVDF layers. The observation that H8DI and H8I are more accurate, respectively, than H8DS and H8S in the PVDF layers is due to the better fulfillment of the mechanical boundary conditions in H8DI and H8I as a result of the enforcement by the incompatible displacement modes, see equation (6). Moreover, the incompatible modes provide a linear thickness variation of the transverse normal stress whereas the assumed

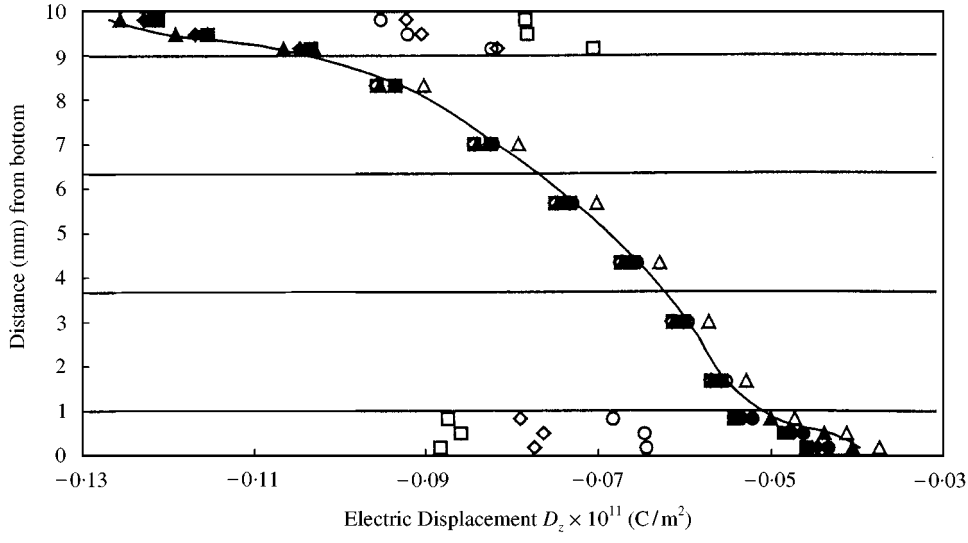

Figure 16. Variation of D_z along AA′ of the simply supported laminated plate under an applied double-sinusoidal mechanical load, see Figure 8: ◇ H8I (4 × 4); □ H8S (4 × 4); △ H8DI (4 × 4); ○ H8DS (4 × 4); ◆ H8I (12 × 12); ■ H8S (12 × 12); ▲ H8DI (12 × 12); ● H8DS (12 × 12); —— analytical [13].

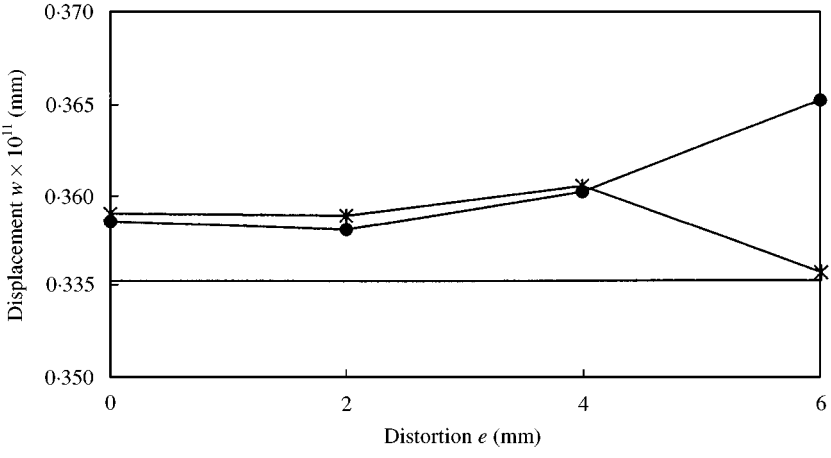

Figure 17. Effect of mesh distortion on the central vertical deflection of the simply supported laminated plate under an applied double-sinusoidal mechanical load, see Figure 11: —●— H8I, H8DI; —∗— H8S, H8DS; —— analytical [13].

transverse normal stress modes in H8S and H8DS are constant w.r.t. the thickness co-ordinate.

The effect of mesh distortion on the predicted central deflection can be seen in Figure 17. The assumed stress elements are more accurate than the incompatible elements.

10. CLOSURE

For piezoelectricity, the irreducible formulation is the one employing independently assumed displacement and electric potential. In this paper, hybrid

eight-node hexahedral finite element models are formulated by employing variational functionals with assumed electric displacement, assumed stress and both. Compared with the irreducible elements, the present hybrid elements are found to be more accurate as well as less sensitive to element distortion and aspect ratio.

ACKNOWLEDGMENT

The work described in this paper was substantially supported by a grant from the Research Grant Council of the Hong Kong SAR, P.R. China (Project No. HKU7082/97E).

REFERENCES

1. H. F. Tiersten 1969 *Linear Piezoelectric Plate Vibration*. New York: Plenum Press.
2. M. C. Ray, K. M. Rao and B. Samanta 1993 *Computers and Structures* **47**, 1031–1042. Exact solution for static analysis of an intelligent structure under cylindrical bending.
3. J. S. Yang, R. C. Batra and X. Q. Liang 1994 *Smart Materials and Structures* **3**, 485–493. The cylindrical bending vibration of a laminated elastic plastic due to piezoelectric actuators.
4. P. R. Heyliger and D. A. Saravanos 1995 *Journal of Acoustical Society of America* **98**, 1547–1557. Exact free-vibration analysis of laminated piezoelectric layers.
5. A. Allik and T. J. R. Hughes 1970 *International Journal of Numerical Methods in Engineering* **2**, 151–157. Finite element method for piezoelectric vibration.
6. M. Naillon, R. Coursant and F. Besnier 1983 *Acta Electronica* **25**, 341–362. Analysis of piezoelectric structures by a finite element method.
7. J. H. Jeng, X. Bao, V. V. Varadan and V. K. Varadan 1988 *Proceedings of IEEE 1988 Ultrasonics Symposium* 685–688. Complete finite element-eigenmode analysis for a 1–3 type of piezoelectric composite transducer including the effect of fluid loading and internal losses.
8. R. Lerch 1990 *IEEE Transactions on Ultrasonics, Ferroelectrics and Frequency Control* **37**, 223–247. Simulation of piezoelectric devices by two- and three-dimensional finite elements.
9. J. A. Hossack and G. Hayward 1991 *IEEE Transactions in Ultrasonics, Ferroelectrics and Frequency Control* **38**, 618–627. Finite-element analysis of 1–3 composite transducers.
10. N.-Q. Guo, P. Cawley and D. Hitchings 1992 *Journal of Sound and Vibration* **159**, 115–138. The finite element analysis of the vibration characteristics of piezoelectric disks.
11. W.-S. Hwang and H. C. Park 1993 *American Institute of Aeronautics and Astronautics Journal* **31**, 930–937. Finite element modeling of piezoelectric sensors and actuators.
12. M. A. Moetakef, K. L. Lawerence, S. P. Joshi and P. S. Shiakolas 1995 *American Institute of Aeronautics and Astronautics Journal* **33**, 136–142. Closed form expressions for higher order electroelastic tetrahedral elements.
13. P. Heyliger, G. Ramirez and D. Saravanos 1994 *Communications and Numerical Methods in Engineering* **10**, 971–981. Coupled discrete-layer finite elements for laminated piezoelectric plates.
14. H. S. Tzou and C. I. Tseng 1990 *Journal of Sound and Vibration* **138**, 17–34. Distributed piezoelectric sensor/actuator design for dynamic measurement/control of distributed parameter systems: a finite element approach.

15. R. Lammering, 1991 *Computers and Structures* **41**, 1101–1109. The application of a finite shell element for composites containing piezo-electric polymers in vibration control.
16. S. K. Ha, C. Keilers and F. K. Chang 1992 *American Institute of Aeronautics and Astronautics Journal* **30**, 772–780. Finite element analysis of composite structures containing distributed piezoceramic sensors and actuators.
17. H. S. Tzou 1993 *Piezoelectric Shells: Distributed Sensing and Control of Continua*. Dordrecht: Kluwer Academic Publishers.
18. H. S. Tzou, C. I. Tseng and H. Bahrami 1994 *Finite Elements in Analysis & Design* **16**, 27–42. A thin piezoelectric hexaxedron finite element applied to design of smart continua.
19. H. S. Tzou and R. Ye 1996 *American Institute of Aeronautics and Astronautics Journal* **34**, 110–115. Analysis of piezoelectric structures with laminated piezoelectric triangle shell element.
20. T. S. Koko, I. R. Orisamolu, M. J. Smith and U. O. Akpan 1997 *Smart Structures and Materials 1997: Mathematics and Control in Smart Structures* (V. V. Varadan, J. Chandra, editors), *Proceedings of SPIE*, **3039**, 125–134. Finite element based design tool for smart composite structures.
21. J. Kim, V. V. Varadan and V. K. Varandan 1997 *International Journal of Numerical Methods in Engineering* **40**, 817–832. Finite element modelling of structures including piezoelectric active devices.
22. D. A. Saravanos, P. R. Heyliger and D. H. Hopkins 1997 *International Journal of Solids and Structures* **34**, 359–378. Layerwise mechanics and finite element for the dynamic analysis of piezoelectric composite plates.
23. O. C. Zienkiewicz and R. L. Taylor 1989 *The Finite Element Method, Vol. 1—Basic Formulation and Linear Problems*. London: McGraw-Hill, fourth edition.
24. R. L. Taylor, P. J. Beresford and E. L. Wilson 1976 *International Journal of Numerical Methods in Engineering* **10**, 1211–1220. A non-conforming element for stress analysis.
25. J. C. Simo and M. S. Rifai 1990 *International Journal of Numerical Methods in Engineering* **29**, 1595–1638. A class of mixed assumed strain methods and the method of incompatible modes.
26. T. H. H. Pian and P. Tong 1969 *International Journal of Numerical Methods in Engineering* **1**, 3–28. Basis of finite elements for solids continua.
27. T. H. H. Pian 1978 *RCA Review* **39**, 648–664. Variational and finite element methods in structural analysis.
28. S. N. Atluri, P. Tong and H. Murakawa 1983 *Hybrid and Mixed Finite Element Methods* (S. N. Atluri, R. H. Gallagher, O. C. Zienkiewicz, editors, 51–71. Chapter 3. Recent studies in hybrid and mixed finite element methods in mechanics.
29. C. A. Felippa 1989 *Communications in Applied Numerical Methods* **5**, 79–98. Parametrized multified variational principles in elasticity: Part I. mixed functionals & Part II. hybrid functionals.
30. T. H. H. Pian 1995 *Finite Elements in Analysis and Design* **21**, 5–20. State-of-the-art development of hybrid/mixed finite element method.
31. T. H. H. Pian and S. W. Lee 1976 *American Institute of Aeronautics and Astronautics Journal* **14**, 824–826. Notes of finite elements for nearly incompressible materials.
32. K. Washizu 1983 *Variational Methods in Elasticity and Plasticity*. Oxford: Pergamon Press, third edition.
33. S. W. Lee and T. H. H. Pian 1978 *American Institute of Aeronautics and Astronautics Journal* **16**, 29–34. Improvement of plate and shell finite elements by mixed formulations.
34. T. H. H. Pian 1985. *Finite Elements in Analysis and Design* **1**, 131–140. Finite elements based on consistently assumed stresses and displacements.
35. S. W. Lee and J. J. Rhiu 1986 *International Journal of Numerical Methods in Engineering* **21**, 1629–1641. A new efficient approach to the formulation of mixed finite elements models for structural analysis.

36. C.-C. Wu, M.-G. Huang and T. H. H. Pian 1987 *Computers and Structures* **27**, 639–644. Consistency condition and convergence criteria of incompatible elements: general formulation of incompatible functions and its application.
37. K. Y. Sze and A. Ghali 1993 *International Journal of Numerical Methods in Engineering* **36**, 1519–1540. Hybrid hexahedral element for solids, plates, shells and beams by selective scaling.
38. K. Y. Sze 1994 *Computer Methods in Applied Mechanical Engineering* **117**, 361–379. An explicit hybrid-stabilized 9-node Lagrangian shell element.
39. K. Y. Sze 1994 *Computer Methods in Applied Mechanical Engineering* **119**, 325–340. Stabilization schemes for 12-node to 21-node brick elements based on orthogonal and consistently assumed stress modes.
40. K. Y. Sze, H. Fan and C. L. Chow 1995 *International Journal of Numerical Methods in Engineering* **38**, 3911–3932. Elimination of spurious kinematic and pressure modes in biquadratic plane element.
41. W.-J. Chen and Y. K. Cheung, *International Journal of Numerical Methods in Engineering* **39**, 2509–2529. Non-conforming element method and refined hybrid method for axisymmetric solids.
42. K. Ghandi and N. W. Hagood 1997 *Smart Structures and Materials 1997: Mathematics and Control in Smart Structures*. (V. V. Varadan, J. Chandra, editors), *Proceedings of SPIE* **3039**, 97–112. A hybrid finite element model for phase transitions in nonlinear electro-mechanically coupled material.
43. E. P. Eernisse 1967 *IEEE Transactions in Sonics and Ultrasonics* **14**, 153–160. Variational method for electrostatic vibration analysis.
44. J. S. Yang 1995 *Quarterly Journal of Applied Mathematics* **53**, 95–104. Variational formulations for the vibration of a piezoelectric body.
45. D. A. Saravanos and P. R. Heyliger 1995 *Journal of Intelligent Material Systems and Structures* **6**, 350–363. Coupled layerwise analysis of composite beams with embedded piezoelectric sensors and actuators.
46. *ABAQUS Theory Manual* 1997 Version 5.6. Rhode Island: Hibbitt, Karlsson & Sorensen Incl.